Macrophage fumarate hydratase restrains mtRNA-mediated interferon production

Macrophage fumarate hydratase restrains mtRNA-mediated interferon production

Alexander Hooftman[1,13]*, Christian G. Peace[1,13], Dylan G. Ryan[1,2,3,13]*, Emily A. Day[1], Ming Yang[2,4], Anne F. McGettrick[1], Maureen Yin[1], Erica N. Montano[5,6], Lihong Huo[5,6], Juliana E. Toller-Kawahisa[1,7], Vincent Zecchini[2], Tristram A.J. Ryan[1], Alfonso Bolado-Carrancio[8], Alva M. Casey[3], Hiran A. Prag[3], Ana S. H. Costa[2,9], Gabriela De Los Santos[5], Mariko Ishimori[5,10], Daniel J. Wallace[5,10], Swamy Venuturupalli[5], Efterpi Nikitopoulou[2], Norma Frizzell[11], Cecilia Johansson[12], Alexander Von Kriegsheim[8], Michael P. Murphy[3], Caroline Jefferies[5,6], Christian Frezza[2,4], Luke A.J. O'Neill[1]*

[1]School of Biochemistry and Immunology, Trinity Biomedical Sciences Institute, Trinity College Dublin
[2]MRC Cancer Unit, University of Cambridge
[3]MRC Mitochondrial Biology Unit, University of Cambridge
[4]Faculty of Medicine, University of Cologne
[5]Department of Medicine, Division of Rheumatology, Cedars-Sinai Medical Center
[6]Department of Biomedical Sciences, Cedars-Sinai Medical Center
[7]Department of Pharmacology, Ribeirao Preto Medical School, University of Sao Paulo
[8]Edinburgh Cancer Research UK Centre, University of Edinburgh
[9]Matterworks, 444 Somerville Ave, Somerville, MA 02143
[10]David Geffen School of Medicine at University of California Los Angeles
[11]School of Medicine Columbia, University of South Carolina
[12]National Heart and Lung Institute, Imperial College London
[13]These authors contributed equally to this work

Summary

Metabolic rewiring underlies macrophage effector functions[1-3], but the mechanisms involved remain incompletely defined. Here, using unbiased metabolomics and stable isotope-assisted tracing, we show induction of an inflammatory aspartate-argininosuccinate shunt following LPS stimulation. The shunt, supported by increased ASS1 expression, also leads to increased cytosolic fumarate levels and fumarate-mediated protein succination. Pharmacologic inhibition and genetic ablation of the TCA cycle enzyme FH further elevates intracellular fumarate levels, suppresses

mitochondrial respiration, and increases mitochondrial membrane potential. RNA sequencing and proteomic analysis demonstrates profound inflammatory effects resulting from FH inhibition. Of note, acute FH inhibition suppresses IL-10 expression leading to increased TNF-α secretion, an effect recapitulated by fumarate esters. Unexpectedly, FH inhibition, but not fumarate esters, also increases IFN-β production through mechanisms that are driven by mitochondrial RNA (mtRNA) release and activation of the RNA sensors TLR7 and RIG-I/MDA5. This effect is recapitulated endogenously when FH is suppressed following prolonged LPS stimulation. Furthermore, cells from SLE patients also exhibit FH suppression, indicating a potential pathogenic role for this process in human disease. We therefore identify a protective role for FH in maintaining appropriate macrophage cytokine and interferon responses.

Keywords

Macrophage, LPS, cytokines, type I interferon, mitochondria, metabolism, mitochondrial retrograde signalling, fumarate hydratase, aspartate-argininosuccinate shunt, fumarate, TNF-α, IL-10, SLE, mtRNA, TLR7, RIG-I, MDA5, antiviral signalling

Main Text

Stimulation of macrophages with the TLR4 ligand lipopolysaccharide (LPS) induces metabolic reprogramming involving rewiring of the TCA cycle and mitochondrial respiration, facilitating cytokine production. Changes in macrophage metabolism have emerged as a major regulator of inflammation[2,4-6]. While metabolic reprogramming is crucial for macrophage activation[7], the players involved and how they regulate cytokine production remain incompletely characterised.

Accumulation of fumarate in macrophages

To evaluate metabolic alterations that occur during LPS stimulation, we employed an unbiased liquid chromatography-mass spectrometry (LC-MS)-based metabolomics approach to characterise the metabolome of inflammatory bone marrow-derived macrophages (BMDMs). The TCA cycle metabolite fumarate stood out as one of the most significantly upregulated metabolites upon exposure to acute LPS stimulation, joining previously identified metabolites such as itaconate[2] (Fig. 1a). We also observed

a significant increase in fumarate-mediated protein succination[8-10], resulting in the formation of the fumarate-cysteine adduct, (S)-2-succinocysteine (2SC) (Extended Data Fig. 1a-c).

As acute LPS stimulation failed to impair respiration (Fig. 1b, c), TCA cycle disruption is unlikely to be sufficient for fumarate accumulation. Increased flux through the aspartate-argininosuccinate shunt has been reported to support nitric oxide (NO) production[5]. As fumarate is a by-product of argininosuccinate cleavage by argininosuccinate lyase (ASL) in the cytosol, we hypothesised that argininosuccinate may be a source of fumarate. Supporting this, we observed decreased aspartate, the substrate for argininosuccinate, and increased argininosuccinate, fumarate, and malate levels (Fig. 1d), consistent with increased flux through the shunt. This rewiring also occurred during prolonged LPS stimulation (Extended Data Fig. 1d).

Argininosuccinate synthase *(Ass1)* and fumarate hydratase (*Fh1*) expression increased and decreased respectively in LPS-stimulated BMDMs, as determined by RT-qPCR (Fig.1e). Using available quantitative proteomics data[2,11], we found argininosuccinate synthase (ASS1) to be upregulated, whereas levels of glutamic-oxaloacetic transaminase 2 (GOT2), ASL and FH were not significantly altered (Fig. 1f). FH protein levels were suppressed only at later time points of LPS (Fig. 1g), indicating that ASS1 induction is vital to the acute accumulation of fumarate.

Inhibition of the aspartate-argininosuccinate shunt with the GOT2 inhibitor aminooxyacetic acid (AOAA)[5] reduced aspartate, asparagine, argininosuccinate and fumarate levels following LPS stimulation (Fig. 1h and Extended Data Fig. 1e). Knockdown of *Asl* also prevented fumarate accumulation (Extended Data Fig. 1f, g) indicating its dependency on the aspartate-argininosuccinate shunt, which would increase cytosolic fumarate (Fig. 1i). With stable isotope-assisted tracing, we show that glutamine-dependent anaplerosis is in part responsible for fumarate accumulation and drives the aspartate-argininosuccinate shunt. U-^{13}C-glutamine tracing demonstrated glutaminolysis as a carbon source for the TCA cycle, aspartate-argininosuccinate shunt metabolites, including fumarate, and glutathione (Extended Data Fig. 2). $^{15}N_2$-glutamine tracing also demonstrated that glutamine nitrogen is a source for glutathione synthesis and aspartate-argininosuccinate shunt metabolites

(Extended Data Fig. 3). Importantly, AOAA completely prevented the contribution of glutamine nitrogen to aspartate, asparagine, arginine and citrulline, confirming its inhibition of GOT2. Metabolomics on cytosolic fractions of resting and LPS-stimulated macrophages showed that metabolites such as itaconate and succinate accumulate in the cytosol following LPS stimulation (Extended Data Fig. 4a). Importantly, we also found increased cytosolic argininosuccinate, fumarate and 2SC (Extended Data Fig. 4b).

We hypothesised that *Irg1*$^{-/-}$ BMDMs (which are unable to synthesise itaconate) would relieve inhibition of succinate dehydrogenase (SDH)[4,12] and exhibit greater accumulation of aspartate-argininosuccinate shunt metabolites. Metabolomics in *Irg1*$^{-/-}$ BMDMs revealed the expected decrease in itaconate and succinate, and increased aspartate-argininosuccinate shunt metabolites, including fumarate and NO (Extended Data Fig. 4c, d), providing further evidence linking mitochondrial TCA cycle activity to an aspartate-argininosuccinate shunt (Extended Data Fig. 4e).

FH inhibition causes metabolic rewiring

FH catalyses the hydration of fumarate to malate in the mitochondrion and cytosol[13], the inhibition of which elevates cytosolic fumarate accumulation, perturbs urea cycle metabolism and leads to renal cyst development[14]. Given protein levels of FH remain stable during early LPS stimulation (Fig. 1g), we used a well-established pharmacological inhibitor of FH (FHIN1)[15] and a recently developed tamoxifen-inducible CRE-ERT2-*Fh1*$^{-/-}$ model to probe the role of FH activity and fumarate accumulation in macrophages. However, since FH inhibition may lead to effects independent of fumarate accumulation through mitochondrial and redox stress[16], we also used low concentrations of cell-permeable dimethyl fumarate (DMF) to deliver a cysteine-reactive fumarate ester which does not inhibit respiration[17-19]. This approach would uncouple the role of impaired mitochondrial bioenergetics following TCA cycle disruption and fumarate-mediated electrophilic modification of cysteine residues.

Previous reports show that immunometabolites and their derivatives affect macrophage function through regulation of metabolic pathways[9,20,21]. We therefore aimed to assess how FH inhibition and DMF may regulate macrophage metabolism. First, comparing the effects of FHIN1 and DMF on mitochondrial bioenergetics, we

found that FHIN1 reduced ratios of ATP/ADP, ATP/AMP, and P-creatine/creatine while DMF had no effect, demonstrating that FH sustains mitochondrial bioenergetics (Fig. 2a, Extended Data Fig. 5a). This was confirmed by respirometry, showing FHIN1 impaired basal respiration, ATP production and maximal respiration as measured by OCR, while DMF had no effect (Fig. 2b). FHIN1 led to a distinct metabolic signature characterised by alterations in TCA cycle metabolites including citrate, aconitate, itaconate and succinate, indicating TCA cycle rewiring, as well as enhanced fumarate and 2SC accumulation, supporting this approach in studying the roles of FH in macrophages (Fig. 2c, e, Extended Data Fig. 5b). Principal component analysis (PCA) showed a significant divergence of FHIN1 treatment to the other conditions (Fig. 2d).

Tamoxifen-inducible knockout of *Fh1* in macrophages (Extended Data Fig. 5c, d) induced similar bioenergetic changes to FHIN1, demonstrated by reduced ATP/AMP and P-creatine/creatine ratios, although the ATP/ADP ratio was unchanged (Extended Data Fig. 5e). TCA cycle rewiring was also observed in *Fh1*$^{-/-}$ macrophages, although to a lesser extent than with FHIN1 (Extended Data Fig. 5f). Compensatory remodelling during initial genetic inactivation of FH may buffer some of the acute changes observed with FHIN1[22]. Importantly however, fumarate and 2SC levels were increased in *Fh1*$^{-/-}$ macrophages (Fig. 2f, Extended Data Fig. 5g), supporting our parallel use of FHIN1 and *Fh1*$^{-/-}$ macrophages.

Confirming previous reports[9], DMF, and to a lesser extent FHIN1, suppressed glycolysis (Extended Data Fig. 5h). GAPDH is reportedly inhibited by fumarate-mediated succination[9,23]. Consistently, FHIN1 increased the glyceraldehyde 3-phosphate (G3P)/2/3-phosphoglycerate (2/3-PG) ratio (Extended Data Fig. 5i), suggesting that endogenous fumarate accumulation may impair GAPDH activity. This provides further evidence that FH impairment leads to modulation of cytosolic processes.

As FHIN1 impaired respiration, we examined further mitochondrial parameters. We first observed increased reactive oxygen species (ROS) production in cells treated with FHIN1 but not DMF (Fig. 2g). FHIN1 treatment also increased staining intensity of the mitochondrial membrane potential (MMP)-dependent dye mitotracker RED (mtRED) (Extended Data Fig. 5j, k). Tetramethylrhodamine methyl ester (TMRM)

staining confirmed this result, as FHIN1 significantly increased staining while DMF had no effect (Fig. 2h). Similarly, *Fh1*$^{-/-}$ macrophages had increased MMP, as previously reported in kidney epithelial cells[24] (Fig. 2h). We also observed a decreased aconitate/citrate ratio in FHIN1-treated macrophages, indicative of impairment in the fumarate- and redox-sensitive TCA cycle enzyme aconitase[25] (Fig. 2i). Although the GSSG/GSH ratio was unchanged, FHIN1 led to a depletion of total glutathione (Fig. 2j), consistent with fumarate-mediated glutathione depletion[26,27]. These data suggest that FH inhibition induces profound redox stress responses.

FH maintains appropriate cytokine responses

To determine whether FH regulates macrophage activation and effector responses, we performed RNA sequencing and proteomics to assess changes in the transcriptome and proteome of FHIN1-treated BMDMs. Geneset enrichment analysis (GSEA) identified an expected suppression in genes associated with metabolism, but FHIN1 also decreased expression of inflammatory pathways, including IL-1 and IL-10 signalling (Fig. 3a). Increased expression of the heme-regulated inhibitor (HRI) stress response, amino acid metabolism and tRNA aminoacylation was also observed (Fig. 3a), consistent with previous reports[16]. Further overrepresentation analysis (ORA) of RNAseq data revealed TNF-α signalling to be the most highly upregulated pathway in our analysis (Fig. 3b).

Comparing FHIN1 with DMF on cytokine readouts allowed us to determine the role of protein succination following FH inhibition. Validating our transcriptomic analysis, FHIN1 and DMF decreased IL-10 release and expression, while TNF-α release and expression were increased (Fig. 3c, Extended Data Fig. 6a). Both compounds also reduced IL-1β expression and IL-6 release (Extended Data Fig. 6b), consistent with previous reports[10,28], demonstrating widespread regulation of cytokine expression.

The less electrophilic fumarate ester, monomethyl fumarate (MMF), exhibited the same effects on *Il10* and *Tnfa* expression (Fig. 3d), supporting a role for their regulation by fumarate. Shared transcriptomic changes of FHIN1 and DMF demonstrated strong downregulation of the ERK1/2 cascade and PI3K signalling (Fig. 3e). A similar transcriptional fingerprint has been observed in FH-deficient leiomyomas[29]. We also observed increased amino acid metabolism and transport, and

autophagy transcripts (Extended Data Fig. 6c). Upon LPS stimulation, IL-10 is regulated by ERK1/2 and PI3K-induced AP-1 activation[30], suggesting that downregulation of this signalling axis by FHIN1 and DMF may repress IL-10. However, we did not observe changes in the upstream kinases (AKT, JNK, ERK and p38) which converge on AP-1 activation, (Extended Data Fig. 6d). Although we did observe reduced *Jun* expression in our transcriptomics dataset (Extended Data Fig. 6e), this could indicate reduced autoregulation by AP-1[31]. In this dataset, *Fos* was not reduced (Extended Data Fig. 6f).

Interestingly, the thiol precursor N-acetyl cysteine (NAC) abrogated the suppression of *Il10* by FHIN1 and DMF (Fig. 3f). The free thiols of NAC and its products would react with and sequester fumarate, thereby reducing the modification of protein thiols and suggesting that suppression of IL-10 results from a redox-dependent succination event. The electrophile sulforaphane has been shown to reduce AP-1 activation via modification of Cys-154 on c-Fos[32]. We therefore investigated if FHIN1 or DMF may affect c-Fos activation, despite upstream regulators remaining unaffected. Using a c-Fos transcription factor assay, we found that FHIN1 and DMF strongly impaired c-Fos activation (Fig. 3g), providing evidence of direct regulation of c-Fos, potentially through S-alkylation.

IL-10 signalling has been shown to repress TNF-α expression[33]. We confirmed this using an IL-10 receptor (CD210) blocking antibody targeting IL-10-mediated STAT3 phosphorylation, leading to augmented LPS-induced TNF-α release (Fig. 3h, Extended Data Fig. 6g). We then examined whether recombinant IL-10 supplementation could rescue the increase in TNF-α. Indeed, with IL-10, FHIN1 failed to impair STAT3 phosphorylation or augment TNF-α production (Fig. 3i, j), indicating that the FHIN1- and DMF-driven induction of TNF-α is dependent on the suppression of IL-10.

Confirming the role of FH in regulating this axis, inducible deletion of *Fh1* in macrophages from heterozygous $Fh1^{+/-}$ or homozygous $Fh1^{-/-}$ mice (Extended Data Fig. 5c, d, Extended Data Fig. 6h) resulted in decreased IL-10 expression and release (Fig. 3k) and increased TNF-α release (Fig. 3l). Furthermore, FHIN1 also suppressed *IL10* expression and increased *TNFA* expression in LPS-stimulated human peripheral

blood mononuclear cells (PBMCs) (Fig. 3m) and macrophages (Fig. 3n), indicating that the FH-regulated IL-10/TNF-α axis is also active in human cells. Establishing the role of LPS-driven fumarate accumulation on release of these cytokines, AOAA, which reduces fumarate accumulation (Fig. 1h), modestly increased and reduced IL-10 and TNF-α release respectively (Extended Data Fig. 6i), indicating that an increase in ASS1, which results in fumarate accumulation, mildly regulates IL-10 and TNF-α production. These effects are accentuated by pharmacological or genetic inhibition of FH, leading to increased fumarate accumulation (Extended Data Fig. 6j). Therefore, sustained expression and activity of FH may be viewed as protective against excessive fumarate accumulation and dysregulated production of IL-10 and TNF-α.

FH inhibition also resulted in the activation of an NRF2 and ATF4 stress response in macrophages (Extended Data Fig. 7a), in line with previous observations in epithelial cells[16]. Proteomic analysis revealed that the inflammation-associated hormone GDF15[34-36] is one of the most significantly increased proteins with FHIN1 and DMF, while FHIN1 also increased the recently identified mitochondrial glutathione importer, SLC25A39[37], reinforcing the mitochondrial redox perturbation (Extended Data Fig. 7b, c). Validating our proteomics data, FH inhibition drove GDF15 release from macrophages (Extended Data Fig. 7d). Both ATF4 and NRF2 have been reported to regulate GDF15 in different contexts[35,38], and silencing of each revealed that FHIN1-driven GDF15 release was partly NRF2- but not ATF4-dependent (Extended Data Fig. 7e, f). This work defines two previously unappreciated signalling axes linked to FH inhibition, uncovering its role in the regulation of IL-10/TNF-α and GDF15. The recent developments identifying GDF15 as a mediator of immune tolerance, and the anti-inflammatory properties of colchicine and NSAIDS[38,39], suggest that protective effects of DMF in models of inflammation could be via GDF15. Additionally, increased TNF-α levels potentially explain adverse events reported with fumarate esters[40]. Mechanistically, suppression of IL-10 may also explain why fumarate esters promote enhanced TNF-α production during trained immunity, in addition to reported epigenetic changes[41].

FH restrains mtRNA-driven IFN-β release

RNAseq analysis of type I interferon (IFN) response genes revealed divergent effects on IFN expression and signalling with FH inhibition, including an upregulation in *Ifnb1* (IFN-β) expression and several interferon-stimulated genes (ISGs), such as *Irf1*, *Ifih1, Rsad2* and *Ifit2* (Fig. 4a). However, other ISGs, such as *Lcn2*, were suppressed by FHIN1 and DMF treatment (Fig. 4a & Extended Data Fig. 8a). Examination of specific type I IFN signalling components downstream of the interferon-α/β receptor (IFNAR) revealed that both FHIN1 and DMF treatment limited IFN-β-induced signal transducer and activator of transcription 1 (STAT1) and Janus kinase 1 (JAK1) phosphorylation (Extended Data Fig. 8b), indicating modest suppression of JAK/STAT signalling. Activation of NRF2 by fumarate and derivatives (Extended Data Fig. 7) may be responsible[42]. Indeed, *Ifnb1* expression was increased with FHIN1 and DMF following *Nrf2* silencing (Extended Data Fig. 8c, d), suggesting that Nrf2 restrains interferon transcription.

Strikingly, FHIN1, but not DMF or MMF, was found to increase IFN-β release from LPS-stimulated macrophages (Fig. 4b, c). This was independent of NAC-sensitive redox stress (Extended Data Fig. 8e), and was not due to augmented TLR4 signalling, as LPS-induced TRAF3 levels and IL-1β expression were not increased by FHIN1 (Extended Data Fig. 8f, g). FHIN1 and DMF did modestly augment LPS-induced p65 phosphorylation (Extended Data Fig. 8h), which may contribute to increased TNF-α release[43]. Given FH inhibition causes mitochondrial stress (Fig. 2) which is associated with the release of immunostimulatory mitochondrial nucleic acids[44-46], we hypothesised that the IFN response was driven by cytosolic nucleic acid sensors, such as cGAS. To support this, FH deficient-hereditary leiomyomatosis and renal cell cancer (HLRCC) tumours exhibit changes in mitochondrial DNA (mtDNA)[22]. We first used ethidium bromide (EtBr) to deplete mtDNA[47] (Extended Data Fig. 8i) before treating cells with FHIN1 and LPS. We found that FHIN1 no longer boosted LPS-induced IFN-β release in the presence of EtBr (Fig. 4d), indicating that increased IFN-β release with FHIN1 may be mtDNA-dependent. We subsequently found that FHIN1 caused an increase in both mtDNA and mtRNA in cytosolic extracts (Fig. 4e, Extended Data Fig. 8j). Given the established role of mtDNA in driving IFN responses[44,45], we examined whether the cGAS-STING or TLR9 DNA-sensing pathways were required for the increase in IFN-β. However, neither use of the STING inhibitor C-178[48] nor

silencing of *Cgas* (cGAS) or *Tmem173* (STING) had any effect on FHIN1-driven IFN-β induction (Extended Data Fig. 8k-n). Targeting TLR9 using the competitive inhibitor ODN 2088[49] or using siRNA also had no effect on this response (Extended Data Fig. 8k-n). Suppression of *Tmem173* expression by FHIN1 and DMF (Extended Data Fig. 8o) may explain why cGAS-STING signalling is redundant in our model, even in the presence of cytosolic mtDNA. ETC inhibition, as we observe with FHIN1 treatment, has also been shown to inhibit STING activation[50].

Since cytosolic mtRNA was also increased by FHIN1 (Fig. 4e), we performed immunofluorescence staining with an antibody specific for double-stranded RNA (dsRNA). Mitochondrial RNA has previously been shown to drive an IFN response in human cells[51,52], and is known to be particularly immunostimulatory[53]. FHIN1 treatment led to an accumulation of dsRNA relative to DMSO control (Fig. 4f). We subsequently co-treated cells with FHIN1 and IMT1, the mitochondrial RNA polymerase (POLRMT) inhibitor. The increase in mtRNA with FHIN1 was observed in the cytosolic fraction but not in the whole cell fraction and was inhibited in both by co-treatment with IMT1 (Extended Data Fig. 8p, q). Importantly, IMT1 also abrogated the FHIN1-mediated boost in IFN-β release (Extended Data Fig. 8r), implicating the role of mtRNA in driving this response. Mitochondrial ssRNA, resulting from a decline in mitochondrial integrity, has also been implicated in driving TLR7-dependent IFN signalling[54,55]. We subsequently silenced *Tlr7* or the dsRNA sensors *Ddx58* (RIG-I) and *Ifih1* (MDA5) (Extended Data Fig. 9a, b), all of which abrogated the boost in IFN-β release observed with FH inhibition (Fig. 4g, h), confirming a non-redundant requirement of these sensors and mtRNA, rather than mtDNA, for the FHIN1-driven IFN response. Knockdown of the cell surface dsRNA sensor *Tlr3* did not affect the augmentation in IFN-β release (Extended Data Fig. 9c). RIG-I and MDA5, although predominantly described as dsRNA sensors, can also bind ssRNA[56], indicating that the IFN response following FH inhibition is likely driven by a mixture of dsRNA and ssRNA species. It is notable that FHIN1 also reduced *Ddx58* but not *Ifih1* expression, which may warrant further investigation (Extended Data Fig. 9b). The signalling events downstream of RIG-I/MDA5 activation include mitochondrial antiviral signalling protein (MAVS) oligomerisation, followed by recruitment and phosphorylation of TANK-binding kinase 1 (TBK1). We observed MAVS oligomerisation and increased TBK1

phosphorylation with FHIN1 treatment (Fig. 4i, Extended Data Fig. 9d). Intriguingly, MAVS knockout did not impair the induction of IFN-β by FHIN1 (Extended Data Fig. 9e), perhaps indicating that compensatory TLR7 signalling is sufficient to drive type I IFN following FH inhibition with chronic MAVS deficiency.

Previously, we demonstrated that FH inhibition causes mitochondrial stress (Fig. 2). Changes in MMP have previously been correlated with increased type I IFN release[57], thus we hypothesised that disturbances in MMP may be linked to mtRNA release and IFN-β induction following FH inhibition. To support this, we induced changes in MMP by using the ATP synthase inhibitor oligomycin A, which boosted MMP, the K^+ ionophore valinomycin A, which non-significantly reduced MMP, or the uncoupler CCCP, which significantly dissipated MMP (Extended Data Fig. 9f, h). All treatments boosted LPS-driven IFN-β release, akin to FHIN1 (Extended Data Fig. 9g, h). MMF, which does not increase LPS-induced IFN-β expression (Fig. 4c), did not affect MMP (Extended Data Fig. 9i). Oligomycin treatment led to an accumulation of dsRNA to a similar extent to that observed in cells treated with FHIN1 or transfected with dsRNA (poly (I:C)), and increased mtRNA release into the cytosol (Extended Data Fig. 9j-l). Valinomycin treatment similarly drove dsRNA accumulation (Extended Data Fig. 9m, n), indicating that MMP-altering compounds induce an accumulation of mtRNA. As we also observed an increase in cytosolic mtDNA levels following oligomycin treatment (Extended Data Fig. 9l), it is still possible that IFN responses following oligomycin/valinomycin/CCCP treatment are not exclusively driven by mtRNA. mtRNA release from chondrocytes has recently been implicated in activating the immune response and promoting osteoarthritis[58]. As such, mitochondrial damage and nucleic acid release are emerging as key pathogenic processes that may underlie many immune-mediated diseases.

Tamoxifen-inducible *Fh1*$^{-/-}$ BMDMs released more IFN-β upon LPS stimulation than their *Fh1*$^{+/+}$ counterparts (Fig. 4j). We also detected increased dsRNA accumulation in *Fh1*$^{-/-}$ BMDMs (Fig 4k, Extended Data Fig. 9o) which, coupled with the fact that deletion of *Fh1* also drives mitochondrial membrane hyperpolarisation (Fig. 2h), demonstrate that both genetic and pharmacological targeting of FH drive similar mitochondrial retrograde type I IFN stress responses.

We next considered whether this response could be applied to an endogenous model of LPS activation in the absence of pharmacological or genetic inactivation of FH. Given LPS-induced FH suppression occurs predominantly during late-phase LPS stimulation (24-48 h) (Fig. 1g), FH suppression at this time point may drive membrane hyperpolarisation and the release of mtRNA. MMP was significantly increased following 48 h LPS stimulation, but not following 4 h or 24 h stimulation (Extended Data Fig. 10a). Although dsRNA did not accumulate following acute (4 h) LPS stimulation (Extended Data Fig. 9j, k), we did observe increased dsRNA staining following 24 h and 48 h LPS stimulation (Extended Data Fig. 10b, c). *Ddx58* and *Ifih1* expression is LPS-inducible (Extended Data Fig. 10d), which may suggest that RIG-I/MDA5 signalling is required during LPS stimulation. Indeed, silencing of *Ddx58* and *Ifih1* reduced both 24 h and 48 h LPS-induced *Ifnb1* expression (Fig. 4l), indicating that *Ifnb1* transcription during late-phase LPS stimulation is maintained by mtRNA release. These results demonstrate that the mitochondrial retrograde type I IFN response, which we initially unmasked by pharmacologically or genetically targeting FH during early LPS signalling, is active endogenously during late-phase LPS activation with potential implications for chronic inflammation, for example during ageing[59].

To determine whether FH inhibition leads to similar effects *in vivo*, we injected mice with FHIN1 or DMF prior to administration of LPS, and measured IFN-β release into the serum. FHIN1 increased LPS-induced IFN-β release, while DMF had no effect (Fig. 4m), indicating that FH inhibition leads to a similar IFN response *in vivo* which may have effects on bystander cells. We also treated human PBMCs with FHIN1 or DMF prior to LPS stimulation and observed similar effects, as FHIN1 boosted, while DMF suppressed LPS-induced IFN-β release (Fig. 4n).

We hereby describe a mitochondrial retrograde signalling pathway leading from FH inhibition to mitochondrial membrane hyperpolarisation and mtRNA release (Supplementary Fig. 1). Mitochondrial stress may be an underlying mechanism that contributes to type I IFN release in interferonopathies such as systemic lupus erythematosus (SLE). It has previously been demonstrated that PBMCs from SLE patients have impaired mitochondrial function and altered MMP[60,61]. We therefore examined *FH* expression in the whole blood of SLE patients and found significant

suppression of *FH* compared to healthy control samples (Fig. 4o). Autoantibodies to dsRNA, as well as dsDNA, have been detected in SLE patients[62,63]. However, it is unclear whether FH suppression is a cause or consequence of increased IFN signalling, as *Fh1* can also be inhibited by IFN-β stimulation in BMDMs (Extended Data Fig. 10e). A negative feedback loop may exist whereby suppression of FH leads to type I IFN release, which feeds back to further suppress FH. FH suppression has previously also been linked to multiple sclerosis progression[64] and, in parallel to our work, has been shown to promote a type I IFN response in kidney epithelial cells and HLRCC tumours (Zecchini, Paupe *et al.,* under revision). This study and ours implicate roles for FH in nucleic acid release, which may contribute to inflammation-driven tumorigenesis and as a potential host defence mechanism in the context of viral infection. Finally, the recent demonstration of aberrant dsRNA editing due to ADAR1 deficiency leading to MDA5 activation as a mechanism of common inflammatory diseases also points to the clinical relevance of endogenously produced dsRNA, suggesting that targeting this pathway may yield novel anti-inflammatory strategies[65].

References (main text)

1 Mills, E. L. *et al.* Succinate Dehydrogenase Supports Metabolic Repurposing of Mitochondria to Drive Inflammatory Macrophages. *Cell* **167**, 457-470 e413, doi:10.1016/j.cell.2016.08.064 (2016).

2 Mills, E. L. *et al.* Itaconate is an anti-inflammatory metabolite that activates Nrf2 via alkylation of KEAP1. *Nature* **556**, 113-117, doi:10.1038/nature25986 (2018).

3 Tannahill, G. M. *et al.* Succinate is an inflammatory signal that induces IL-1beta through HIF-1alpha. *Nature* **496**, 238-242, doi:10.1038/nature11986 (2013).

4 Lampropoulou, V. *et al.* Itaconate Links Inhibition of Succinate Dehydrogenase with Macrophage Metabolic Remodeling and Regulation of Inflammation. *Cell Metab* **24**, 158-166, doi:10.1016/j.cmet.2016.06.004 (2016).

5 Jha, Abhishek K. *et al.* Network Integration of Parallel Metabolic and Transcriptional Data Reveals Metabolic Modules that Regulate Macrophage Polarization. *Immunity* **42**, 419-430, doi:10.1016/j.immuni.2015.02.005 (2015).

6 Billingham, L. K. *et al.* Mitochondrial electron transport chain is necessary for NLRP3 inflammasome activation. *Nat Immunol* **23**, 692-704, doi:10.1038/s41590-022-01185-3 (2022).

7 Mills, E. L., Kelly, B. & O'Neill, L. A. J. Mitochondria are the powerhouses of immunity. *Nat Immunol* **18**, 488-498, doi:10.1038/ni.3704 (2017).

8 Adam, J. *et al.* Renal cyst formation in Fh1-deficient mice is independent of the Hif/Phd pathway: roles for fumarate in KEAP1 succination and Nrf2 signaling. *Cancer Cell* **20**, 524-537, doi:10.1016/j.ccr.2011.09.006 (2011).

9 Kornberg, M. D. *et al.* Dimethyl fumarate targets GAPDH and aerobic glycolysis to modulate immunity. *Science* **360**, 449-453, doi:10.1126/science.aan4665 (2018).

10 Humphries, F. *et al.* Succination inactivates gasdermin D and blocks pyroptosis. *Science*, doi:10.1126/science.abb9818 (2020).

11 Williams, N. C. *et al.* Signaling metabolite L-2-hydroxyglutarate activates the transcription factor HIF-1alpha in lipopolysaccharide-activated macrophages. *J Biol Chem* **298**, 101501, doi:10.1016/j.jbc.2021.101501 (2021).

12 Cordes, T. *et al.* Immunoresponsive Gene 1 and Itaconate Inhibit Succinate Dehydrogenase to Modulate Intracellular Succinate Levels. *J Biol Chem* **291**, 14274-14284, doi:10.1074/jbc.M115.685792 (2016).

13 Sass, E., Blachinsky, E., Karniely, S. & Pines, O. Mitochondrial and cytosolic isoforms of yeast fumarase are derivatives of a single translation product and have identical amino termini. *J Biol Chem* **276**, 46111-46117, doi:10.1074/jbc.M106061200 (2001).

14 Adam, J. *et al.* A role for cytosolic fumarate hydratase in urea cycle metabolism and renal neoplasia. *Cell Rep* **3**, 1440-1448, doi:10.1016/j.celrep.2013.04.006 (2013).

15 Takeuchi, T., Schumacker, P. T. & Kozmin, S. A. Identification of fumarate hydratase inhibitors with nutrient-dependent cytotoxicity. *J Am Chem Soc* **137**, 564-567, doi:10.1021/ja5101257 (2015).

16 Ryan, D. G. *et al.* Disruption of the TCA cycle reveals an ATF4-dependent integration of redox and amino acid metabolism. *Elife* **10**, doi:10.7554/eLife.72593 (2021).

17 Hayashi, G. *et al.* Dimethyl fumarate mediates Nrf2-dependent mitochondrial biogenesis in mice and humans. *Hum Mol Genet* **26**, 2864-2873, doi:10.1093/hmg/ddx167 (2017).

18 Sciacovelli, M. *et al.* Fumarate is an epigenetic modifier that elicits epithelial-to-mesenchymal transition. *Nature* **537**, 544-547, doi:10.1038/nature19353 (2016).
19 Wang, Y. P. *et al.* Malic enzyme 2 connects the Krebs cycle intermediate fumarate to mitochondrial biogenesis. *Cell Metab* **33**, 1027-1041 e1028, doi:10.1016/j.cmet.2021.03.003 (2021).
20 Lampropoulou, V. *et al.* Itaconate Links Inhibition of Succinate Dehydrogenase with Macrophage Metabolic Remodeling and Regulation of Inflammation. **24**, 158-166, doi:10.1016/j.cmet.2016.06.004 (2016).
21 Liao, S. T. *et al.* 4-Octyl itaconate inhibits aerobic glycolysis by targeting GAPDH to exert anti-inflammatory effects. *Nat Commun* **10**, 5091, doi:10.1038/s41467-019-13078-5 (2019).
22 Crooks, D. R. *et al.* Mitochondrial DNA alterations underlie an irreversible shift to aerobic glycolysis in fumarate hydratase-deficient renal cancer. *Sci Signal* **14**, doi:10.1126/scisignal.abc4436 (2021).
23 Blatnik, M., Frizzell, N., Thorpe, S. R. & Baynes, J. W. Inactivation of glyceraldehyde-3-phosphate dehydrogenase by fumarate in diabetes: formation of S-(2-succinyl)cysteine, a novel chemical modification of protein and possible biomarker of mitochondrial stress. *Diabetes* **57**, 41-49, doi:10.2337/db07-0838 (2008).
24 Tyrakis, P. A. *et al.* Fumarate Hydratase Loss Causes Combined Respiratory Chain Defects. *Cell Rep* **21**, 1036-1047, doi:10.1016/j.celrep.2017.09.092 (2017).
25 Ternette, N. *et al.* Inhibition of mitochondrial aconitase by succination in fumarate hydratase deficiency. *Cell Rep* **3**, 689-700, doi:10.1016/j.celrep.2013.02.013 (2013).
26 Sullivan, L. B. *et al.* The proto-oncometabolite fumarate binds glutathione to amplify ROS-dependent signaling. *Mol Cell* **51**, 236-248, doi:10.1016/j.molcel.2013.05.003 (2013).
27 Zheng, L. *et al.* Fumarate induces redox-dependent senescence by modifying glutathione metabolism. *Nat Commun* **6**, 6001, doi:10.1038/ncomms7001 (2015).
28 Bambouskova, M. *et al.* Electrophilic properties of itaconate and derivatives regulate the IkappaBzeta-ATF3 inflammatory axis. *Nature* **556**, 501-504, doi:10.1038/s41586-018-0052-z (2018).
29 Raimundo, N., Vanharanta, S., Aaltonen, L. A., Hovatta, I. & Suomalainen, A. Downregulation of SRF-FOS-JUNB pathway in fumarate hydratase deficiency and in uterine leiomyomas. *Oncogene* **28**, 1261-1273, doi:10.1038/onc.2008.472 (2009).
30 Hu, X. *et al.* IFN-gamma suppresses IL-10 production and synergizes with TLR2 by regulating GSK3 and CREB/AP-1 proteins. *Immunity* **24**, 563-574, doi:10.1016/j.immuni.2006.02.014 (2006).
31 Angel, P., Hattori, K., Smeal, T. & Karin, M. The jun proto-oncogene is positively autoregulated by its product, Jun/AP-1. *Cell* **55**, 875-885, doi:10.1016/0092-8674(88)90143-2 (1988).
32 Dickinson, S. E. *et al.* Inhibition of activator protein-1 by sulforaphane involves interaction with cysteine in the cFos DNA-binding domain: implications for chemoprevention of UVB-induced skin cancer. *Cancer Res* **69**, 7103-7110, doi:10.1158/0008-5472.CAN-09-0770 (2009).

33 de Waal Malefyt, R., Abrams, J., Bennett, B., Figdor, C. G. & de Vries, J. E. Interleukin 10(IL-10) inhibits cytokine synthesis by human monocytes: an autoregulatory role of IL-10 produced by monocytes. *J Exp Med* **174**, 1209-1220, doi:10.1084/jem.174.5.1209 (1991).

34 Luan, H. H. *et al.* GDF15 Is an Inflammation-Induced Central Mediator of Tissue Tolerance. *Cell* **178**, 1231-1244 e1211, doi:10.1016/j.cell.2019.07.033 (2019).

35 Day, E. A. *et al.* Metformin-induced increases in GDF15 are important for suppressing appetite and promoting weight loss. *Nat Metab* **1**, 1202-1208, doi:10.1038/s42255-019-0146-4 (2019).

36 Coll, A. P. *et al.* GDF15 mediates the effects of metformin on body weight and energy balance. *Nature* **578**, 444-448, doi:10.1038/s41586-019-1911-y (2020).

37 Wang, Y. *et al.* SLC25A39 is necessary for mitochondrial glutathione import in mammalian cells. *Nature* **599**, 136-140, doi:10.1038/s41586-021-04025-w (2021).

38 Weng, J. H. *et al.* Colchicine acts selectively in the liver to induce hepatokines that inhibit myeloid cell activation. *Nat Metab* **3**, 513-522, doi:10.1038/s42255-021-00366-y (2021).

39 Eisenstein, A. *et al.* Activation of the transcription factor NRF2 mediates the anti-inflammatory properties of a subset of over-the-counter and prescription NSAIDs. *Immunity* **55**, 1082-1095 e1085, doi:10.1016/j.immuni.2022.04.015 (2022).

40 Asadullah, K. *et al.* Influence of monomethylfumarate on monocytic cytokine formation--explanation for adverse and therapeutic effects in psoriasis? *Arch Dermatol Res* **289**, 623-630, doi:10.1007/s004030050251 (1997).

41 Arts, R. J. *et al.* Glutaminolysis and Fumarate Accumulation Integrate Immunometabolic and Epigenetic Programs in Trained Immunity. *Cell Metab* **24**, 807-819, doi:10.1016/j.cmet.2016.10.008 (2016).

42 Ryan, D. G. *et al.* Nrf2 activation reprograms macrophage intermediary metabolism and suppresses the type I interferon response. *iScience* **25**, 103827, doi:https://doi.org/10.1016/j.isci.2022.103827 (2022).

43 Shanmugasundaram, K. *et al.* The oncometabolite fumarate promotes pseudohypoxia through noncanonical activation of NF-kappaB signaling. *J Biol Chem* **289**, 24691-24699, doi:10.1074/jbc.M114.568162 (2014).

44 West, A. P. *et al.* Mitochondrial DNA stress primes the antiviral innate immune response. *Nature* **520**, 553-557, doi:10.1038/nature14156 (2015).

45 Sliter, D. A. *et al.* Parkin and PINK1 mitigate STING-induced inflammation. *Nature* **561**, 258-262, doi:10.1038/s41586-018-0448-9 (2018).

46 McArthur, K. *et al.* BAK/BAX macropores facilitate mitochondrial herniation and mtDNA efflux during apoptosis. *Science* **359**, doi:10.1126/science.aao6047 (2018).

47 Dang, E. V., McDonald, J. G., Russell, D. W. & Cyster, J. G. Oxysterol Restraint of Cholesterol Synthesis Prevents AIM2 Inflammasome Activation. *Cell* **171**, 1057-1071 e1011, doi:10.1016/j.cell.2017.09.029 (2017).

48 Haag, S. M. *et al.* Targeting STING with covalent small-molecule inhibitors. *Nature* **559**, 269-273, doi:10.1038/s41586-018-0287-8 (2018).

49 Stunz, L. L. *et al.* Inhibitory oligonucleotides specifically block effects of stimulatory CpG oligonucleotides in B cells. *Eur J Immunol* **32**, 1212-1222, doi:10.1002/1521-4141(200205)32:5<1212::AID-IMMU1212>3.0.CO;2-D (2002).

50 Prantner, D. *et al.* 5,6-Dimethylxanthenone-4-acetic acid (DMXAA) activates stimulator of interferon gene (STING)-dependent innate immune pathways and is regulated by mitochondrial membrane potential. *J Biol Chem* **287**, 39776-39788, doi:10.1074/jbc.M112.382986 (2012).

51 Dhir, A. *et al.* Mitochondrial double-stranded RNA triggers antiviral signalling in humans. *Nature* **560**, 238-242, doi:10.1038/s41586-018-0363-0 (2018).

52 Tigano, M., Vargas, D. C., Tremblay-Belzile, S., Fu, Y. & Sfeir, A. Nuclear sensing of breaks in mitochondrial DNA enhances immune surveillance. *Nature* **591**, 477-481, doi:10.1038/s41586-021-03269-w (2021).

53 Kariko, K., Buckstein, M., Ni, H. & Weissman, D. Suppression of RNA recognition by Toll-like receptors: the impact of nucleoside modification and the evolutionary origin of RNA. *Immunity* **23**, 165-175, doi:10.1016/j.immuni.2005.06.008 (2005).

54 Rai, P. *et al.* IRGM1 links mitochondrial quality control to autoimmunity. *Nat Immunol* **22**, 312-321, doi:10.1038/s41590-020-00859-0 (2021).

55 Kruger, A. *et al.* Human TLR8 senses UR/URR motifs in bacterial and mitochondrial RNA. *EMBO Rep* **16**, 1656-1663, doi:10.15252/embr.201540861 (2015).

56 Pichlmair, A. *et al.* RIG-I-mediated antiviral responses to single-stranded RNA bearing 5'-phosphates. *Science* **314**, 997-1001, doi:10.1126/science.1132998 (2006).

57 Koshiba, T., Yasukawa, K., Yanagi, Y. & Kawabata, S. Mitochondrial membrane potential is required for MAVS-mediated antiviral signaling. *Sci Signal* **4**, ra7, doi:10.1126/scisignal.2001147 (2011).

58 Kim, S. *et al.* Mitochondrial double-stranded RNAs govern the stress response in chondrocytes to promote osteoarthritis development. *Cell Rep* **40**, 111178, doi:10.1016/j.celrep.2022.111178 (2022).

59 Rasa, S. M. M. A., F.; Krepelova, A.; Nunna, S.; Omrani, O.; Gebert, N.; Adam, L.; Käppel, S.; Höhn, S.; Donati, G.; Jurkowski, T.P.; Rudolph, K.L.; Ori, A.; Neri, F. Inflammaging is driven by upregulation of innate immune receptors and systemic interferon signaling and is ameliorated by dietary restriction. *Cell Rep* **39** (2022).

60 Buskiewicz, I. A. *et al.* Reactive oxygen species induce virus-independent MAVS oligomerization in systemic lupus erythematosus. *Sci Signal* **9**, ra115, doi:10.1126/scisignal.aaf1933 (2016).

61 Ruiz-Limon, P. *et al.* Atherosclerosis and cardiovascular disease in systemic lupus erythematosus: effects of in vivo statin treatment. *Ann Rheum Dis* **74**, 1450-1458, doi:10.1136/annrheumdis-2013-204351 (2015).

62 Davis, P., Cunnington, P. & Hughes, G. R. Double-stranded RNA antibodies in systemic lupus erythematosus. *Ann Rheum Dis* **34**, 239-243, doi:10.1136/ard.34.3.239 (1975).

63 Caielli, S. *et al.* Oxidized mitochondrial nucleoids released by neutrophils drive type I interferon production in human lupus. *J Exp Med* **213**, 697-713, doi:10.1084/jem.20151876 (2016).

64 Sarkar, P. *et al.* Reduced expression of mitochondrial fumarate hydratase in progressive multiple sclerosis contributes to impaired in vitro mesenchymal stromal cell-mediated neuroprotection. *Mult Scler* **28**, 1179-1188, doi:10.1177/13524585211060686 (2022).

65 Li, Q. *et al.* RNA editing underlies genetic risk of common inflammatory diseases. *Nature*, doi:10.1038/s41586-022-05052-x (2022).

Figure Legends

Figure 1 – LPS stimulation drives fumarate accumulation via glutamine anaplerosis and an aspartate-argininosuccinate shunt

Metabolite abundance (**a,d**) and bioenergetic ratios (**b**) in non-stimulated (NS) versus LPS-stimulated BMDMs (*n* = 3; LPS 4 h; argininosuccinate (P=0.000044), fumarate (P=0.000141), malate (P=0.000219))**. c,** Respirometry as measured by oxygen consumption rate (OCR) of NS and LPS-stimulated BMDMs (*n* = 6 (NS); *n* = 8 (LPS); LPS 4 h). *n* = technical replicates from 1 experiment performed with 3 pooled biological replicates. Data are mean ± s.d. **e**, *Ass1* and *Fh1* gene expression with LPS time-course (*n* = 9; 24 h (P=0.000729), 48 h (P=0.000001)). **f**, Quantitative proteomics of aspartate-argininosuccinate shunt enzymes in NS and LPS-stimulated BMDMs (*n* = 4, LPS 24 h; ASS1 (P=0.000156)). **g,** FH protein levels with LPS time-course (*n* = 1). **h**, Fumarate levels following LPS stimulation with or without aminooxyacetic acid (AOAA) pre-treatment (1 h) (*n* = 6, LPS 4 h)**. i**, Schematic of metabolic changes occurring during early-phase TCA cycle rewiring. Created with BioRender.com. **b,d-f,h,** Data are mean ± s.e.m. *n* = biological replicates unless stated otherwise. *P* values calculated using two-tailed Student's *t*-test for paired comparisons or one-way analysis of variance (ANOVA) for multiple comparisons.

Figure 2 – FH inhibition increases bioenergetic stress, fumarate levels and mitochondrial membrane potential

Bioenergetic ratios (**a**) and heatmap of top 50 differentially abundant metabolites (**c**) in BMDMs pre-treated with vehicle (DMSO), FH inhibitor (FHIN1) or dimethyl fumarate (DMF) (*n* = 3; LPS 4 h; ATP/ADP (P=0.000004), phosphocreatine/creatine (P=0.00000001)). **b**, Respirometry of BMDMs pre-treated with DMSO, FHIN1 or DMF (*n* = 8; LPS 4 h)**.** *n* = technical replicates from 1 experiment performed with 3 pooled biological replicates. Data are mean ± s.d. **d,** PCA plot of metabolomics in BMDMs pre-treated with DMSO, FHIN1 or DMF or (*n* = 3; LPS 4 h). **e**, Fumarate levels in BMDMs pre-treated with DMSO or FHIN1 (*n* = 9; LPS 4 h). **f,** Fumarate and 2SC levels in $Fh1^{+/+}$ and $Fh1^{-/-}$ BMDMs (*n* = 3; 96 h EtOH/TAM; LPS 4 h). **g,** Mean fluorescence intensity (MFI) of CellROX staining in BMDMs pre-treated with DMSO, FHIN1 or DMF (*n* = 3 (CellROX); *n* = 4 (TMRM); LPS 4 h). **h,** MFI of TMRM staining in BMDMs pre-treated with DMSO, FHIN1 or DMF or $Fh1^{+/+}$ and $Fh1^{-/-}$ BMDMs (*n* = 4 (DMSO/FHIN1/DMF); *n* = 3 ($Fh1^{+/+}$ and $Fh1^{-/-}$); 72 h EtOH/TAM; LPS 4 h)**. i,** Aconitate/citrate ratio following LPS stimulation with or without FHIN1 or DMF pre-treatment (*n* = 3; LPS 4 h). **j,** GSH and GSSG levels following LPS stimulation with or without FHIN1 or DMF pre-treatment (*n* = 3; LPS 4 h). **a,e-j** Data are mean ± s.e.m**.** *n* = biological replicates unless stated otherwise. *P* values calculated using two-tailed Student's *t*-test for paired comparisons or one-way or ANOVA for multiple comparisons**.**

Figure 3 – FH activity is required to maintain appropriate cytokine responses

GSEA (**a**) and overrepresentation analysis (ORA) (**b**) of RNAseq in BMDMs pre-treated with FHIN1 or DMSO (*n* = 3; LPS 4 h). **c**, IL-10 and TNF-α release from DMSO- FHIN1- or DMF-pre-treated BMDMs (*n* = 6; LPS 4 h; FHIN1/IL-10 (P=0.0000024), DMF/IL-10 (P=0.0000018), FHIN1/TNF (P=0.000001)). **d**, *Il10* and *Tnfa* expression in DMSO- or MMF-pre-treated BMDMs (*n* = 3; LPS 4 h). **e**, Enrichment map plot of shared significantly decreased genes in FHIN1- and DMF-pre-treated BMDMs (*n* = 3; LPS 4 h). **f**, *Il10* expression in DMSO- FHIN1- or DMF-pre-treated BMDMs in the presence of NAC (*n* = 3; LPS 4 h). **g**, c-Fos activity in DMSO- FHIN1- or DMF-pre-treated BMDMs (*n* = 3; LPS 4 h; DMF (P=0.0000298)). **h,** TNF-α release from BMDMs pre-treated with anti-CD210 antibody (1 h) (*n* = 4; LPS 4 h). Western blot for STAT3 and phospho-STAT3 (**i**) and TNF-α release (**j**) from DMSO- FHIN1- or DMF-pre-treated BMDMs and co-treated with IL-10 (*n* = 3, LPS 4 h; DMF (P=0.000163)). **k,** *Il10* expression and IL-10 release in $Fh1^{+/+}$ and $Fh1^{-/-}$ (*n* = 5 or 2)/$Fh1^{+/-}$ (*n* = 2) BMDMs (EtOH/TAM 72 h; LPS 4 h; *Il10* (P= 0.000055)). **l,** TNF-α release from $Fh1^{+/+}$ and $Fh1^{-/-}$ *(n = 5)*/$Fh1^{+/-}$ *(n = 2)* BMDMs (EtOH/TAM 72 h; LPS 4 h). **m,** *IL10* and *TNFA* expression in DMSO- or FHIN1-pre-treated human PBMCs (*n* = 8, LPS 4 h; FHIN1 (P=0.00000008)). **n,** *IL10* and *TNFA* expression in DMSO- or FHIN1- pre-treated human macrophages (*n* = 3, LPS 4 h; FHIN1 (P=0.000028)). **c,d,f-h,j-n** Data are mean ± s.e.m. **i,** 1 representative blot of 3 shown. *n* = biological replicates. *P* values calculated using two-tailed Student's t-test for paired comparisons or one-way ANOVA for multiple comparisons.

Figure 4 – FH impairment triggers IFN-β release via a mtRNA-driven retrograde response

a, Volcano plot of DMSO- or FHIN1-pre-treated BMDMs (*n* = 3; LPS 4 h). **b**, IFN-β release from DMSO-, FHIN1- or DMF-pre-treated BMDMs (*n* = 6; LPS 4 h; FHIN1 (P=0.000004)). **c**, *Ifnb1* in DMSO- or MMF-pre-treated BMDMs (*n* = 3; LPS 4 h). **d**, IFN-β release from BMDMs treated with EtBr (6 days), before pre-treatment with DMSO or FHIN1 (*n* = 6; LPS 4 h). **e**, Cytosolic *D-loop* in DNA and RNA in DMSO- or FHIN1- pre-treated BMDMs (*n* = 4 for mtDNA, *n* = 5 for mtRNA; LPS 4 h). **f**, dsRNA in DMSO- or FHIN1-pre-treated BMDMs (*n* = 3; LPS 4 h). Scale bar = 20 μm. **g,** *Ifnb1* with *Tlr7* silencing in DMSO- or FHIN1-pre-treated BMDMs (*n* = 3; LPS 4 h). **h**, IFN-β with *Ddx58* or *Ifih1* silencing in DMSO- or FHIN1-pre-treated BMDMs (*n* = 7; LPS 4 h). **i,** MAVS in DMSO- or FHIN1-pre-treated BMDMs (*n* = 3; LPS 4 h). **j**, IFN-β in $Fh1^{+/+}$ and $Fh1^{-/-}$ BMDMs (*n* = 3, EtOH/TAM 72 h; LPS 4 h). **k,** dsRNA in $Fh1^{+/+}$ and $Fh1^{-/-}$ BMDMs (*n* = 3; EtOH/TAM 72 h; LPS 4 h). Scale bar = 20 μm. **l,** *Ifnb1* with *Ddx58* or *Ifih1* silencing (*n* = 3). **m,** Serum IFN-β of FHIN1- or DMF-treated mice prior to PBS or LPS injection (*n* = 5 (PBS); *n* = 10 (FHIN1/LPS); *n* = 11 (Vehicle/LPS); *n* = 12 (DMF/LPS)). **n,** IFN-β release from DMSO-, FHIN1- or DMF-pre-treated human PBMCs (*n* = 3; LPS 4 h). **o,** *FH* in whole blood from healthy controls and SLE patients (*n* = 30; P=0.0000005). **b-e,g,h,j,i-o,** Data are mean ± s.e.m. **f,i,k,** 1 representative blot or image of 3 experiments shown. *n* = biological replicates. *P* values calculated using two-tailed Student's t-test for paired comparisons, one-way ANOVA for multiple comparisons.

Materials and Methods

Animal Details

All mice were on a C57BL/6JOlaHsd background unless stated below. Wild-type (WT) mice were bred in-house. The inducible *Fh1*$^{+/fl}$ and *Fh1*$^{fl/fl}$ mice were generated on the C57BL/6 genetic background and their hind legs were generously donated by Dr. Christian Frezza (University of Cambridge, UK). Vehicle (ethanol) treated *Fh1*$^{+/+}$ and *Fh1*$^{-/l}$ were used as controls. Upon treatment with 4-hydroxy tamoxifen, Cre-mediated chromatin excision results in the loss of either one (*Fh1*$^{+/-}$) or both (*Fh1*$^{-/-}$) copies of *Fh1*, thus generating either heterozygous or null animals. Hind legs from WT and *Mavs*$^{-/-}$ mice were generously donated by Dr Cecilia Johansson (Imperial College London, UK). These strains, originally obtained from S. Akira (World Premier International Immunology Frontier Research Center, Osaka University, Osaka, Japan), were *Ifna6*$^{gfp/+}$ but since *Ifna6* expression was not a primary readout the mice are designated as WT and *Mavs*$^{-/-}$. *In vitro* experiments were performed with BMDMs isolated from 6-18-week-old female and male mice. Although we did not use statistical methods to calculate sample size, we decided to use a minimum of 3 biological replicates per experiment to account for biological variability, considering the 3 Rs principle and the fact that most experiments were performed in primary murine macrophages from inbred mice. All *in vitro* treatment groups were randomly assigned. *In vitro* and *in vivo* experiments were not blinded due to lack of available experimenters with required expertise. *In vivo* models were performed with 6-week-old male mice and littermates were randomly assigned to experimental groups. Animals were maintained under specific pathogen-free conditions in line with Irish and European Union regulations. All animal procedures were ethically approved by the Trinity College Dublin Animal Research Ethics Committee prior to experimentation and conformed with the Directive 2010/63/EU of the European Parliament.

Generation of Murine BMDMs

6-18-week-old mice were euthanised in a CO_2 chamber, and death was confirmed by cervical dislocation. Bone marrow was subsequently harvested from the tibia, femur and ilium and cells were differentiated in DMEM containing L929 supernatant (20%), foetal calf serum (FCS) (10%), and penicillin/streptomycin (1%) for 6 days, after which

cells were counted and plated at 0.5 x 10^6 cells/ml unless otherwise stated. BMDMs were plated in 12-well cell culture plates and left overnight to adhere.

Isolation of Human PBMCs

Human blood samples from healthy donors were collected and processed at the School of Biochemistry and Immunology in TBSI (TCD). Blood samples were obtained anonymously and written informed consent for the use of blood for research purposes has been obtained from the donors. All the procedures involving experiments on human samples have been approved by the School of Biochemistry and Immunology Research Ethics Committee (TCD). Experiments were conducted according to the TCD guide on good research practice, which follows the guidelines detailed in the National Institutes of Health Belmont Report (1978) and the Declaration of Helsinki. 30 ml whole blood was layered on 20 ml Lymphoprep (Axis-Shield), followed by centrifugation for 20 mins at 400 x g with the brake off, after which the upper plasma layer was removed and discarded. The layer of mononuclear cells at the plasma-density gradient medium interface was retained, and 20 ml PBS was added. Cells were centrifuged for 8 mins at 300 x g and the resulting supernatant was removed and discarded. The remaining pellet of mononuclear cells was resuspended, counted, and plated at 1 x 10^6 cells/ml in RPMI supplemented with FCS (10%) and penicillin/streptomycin (1%).

Generation of Human Macrophages

PBMCs were taken, and CD14+ monocytes were isolated using MagniSort Human CD14 Positive Selection Kit (Thermo Fisher) according to the manufacturer's protocol. CD14 Monocytes were then differentiated in T-175 flasks in RPMI containing FCS (10%), penicillin/streptomycin (1%) and recombinant human M-CSF (1:1000). After 6 days, the supernatant was discarded, cells were scraped and counted, and human monocyte-derived macrophages (hMDMs) were plated in 12-well plates at 1 x 10^6 cells/mL RPMI containing FCS (10%) and penicillin/streptomycin (1%).

Whole Blood Isolation from SLE Patients

All SLE patients (as per ACR diagnostic criteria) were recruited from Cedars-Sinai Medical Center, CA, USA. Age- and sex-matched healthy donors who had no history of autoimmune diseases or treatment with immunosuppressive agents were included.

All participants provided informed written consent and the study received prior approval from the institutional ethics review board (IRB protocol. 19627). Blood was collected into PAXgene RNA tubes (2.5 mL blood + 6.9 mL buffer) and stored at -80°C. Before isolation of RNA, the tubes were thawed at room temperature for 16 h. Total RNA was isolated using the PAXgene Blood RNA Kit according to manufacturer's recommendations (PreAnalytiX GmbH, 08/2005, REF: 762174).

Reagents

LPS from *Escherichia coli*, serotype EH100 (ALX-581-010-L001), was purchased from Enzo Life Sciences. High molecular weight poly (I:C) (tlrl-pic) and 2'-3'-cGAMP (tlrl-nacga23) were purchased from Invivogen. Recombinant mouse IFN-β1 (581302) and recombinant mouse IL-10 (417-ML-005/CF) were purchased from Biolegend. ATP disodium salt (A2383), dimethyl sulfoxide (DMSO) (D8418), aminooxyacetic acid (AOAA) (C13408), valinomycin (V3639), 4-hydroxytamoxifen (H6278) and N-acetyl cysteine (NAC) (A7250) were purchased from Sigma Aldrich. Oligomycin A from *Streptomyces diastatochromogenes* (M02220) was purchased from Fluorochem. Fumarate hydratase-IN-1 (FHIN1) (HY-100004), dimethyl fumarate (DMF) (HY-17363), monomethyl fumarate (MMF) (HY-103252), IMT1 (HY-134539) and C-178 (HY-123963) were purchased from MedChemExpress. CPG ODN 1826 (130-100-274) and ODN 2088 (130-105-815) were purchased from Miltenyi Biotec. CCCP (M20036) was purchased from Thermo Fisher.

Compound Treatments

All compounds used DMSO as a vehicle except for 4-hydroxy tamoxifen (EtOH), NAC (PBS), and AOAA for tracing experiments (Media). LPS was used at a concentration of 100 ng/mL for indicated timepoints (2, 3, 4, 6, 8, 24, 48 h). FHIN1 (10 or 20 μM), MMF (50 or 100 μM), DMF (25 μM), AOAA (5 mM), oligomycin (10 μM), CCCP (50 μM) NAC (1 mM), and IMT1 (10 μM) pre-treatments were performed for 3 h prior the addition of LPS. Cells were treated with valinomycin (10 nM) 15 mins before LPS stimulation. Anti-CD210 or IgG control (10 μg/ml) antibodies were added to cells 1 h prior to LPS stimulation. Recombinant mouse IL-10 protein (100 ng/ml) was added to cells at the same time as LPS. Cells were treated with IFN-β1 (220 ng/ml) for 3 h. Cells were treated with C-178 (1 μM) 1 h prior to LPS stimulation or transfection with 2'3'-cGAMP (1.5 μg/ml) for 4 hrs to achieve cGAS-STING activation. Cells were treated

with ODN 2088 (1 μM) for 1 hr prior to LPS stimulation or transfection with CPG ODN 1826 (1.5 μg/ml) to achieve TLR9 activation. 3 different timepoints of 4-hydroxy tamoxifen (TAM) (600 nM or 2 μM) or EtOH treatment were performed- these are specified in the individual figure legends. For '48 h' treatments EtOH/TAM was added on day 5 of 6 during the BMDM differentiation protocol. On day 6 they were plated with EtOH/TAM (left overnight) and treated the following day. For '72 h' treatments EtOH/TAM was added on day 4 of 6 during the BMDM differentiation protocol. On day 6 they were plated with EtOH/TAM (left overnight) and treated the following day. For '96 h' treatments EtOH/TAM was added on day 4 of 6 during the BMDM differentiation protocol. On day 6 they were plated with EtOH/TAM and treated 2 days later.

Antibodies

Working dilutions of antibodies were 1/1000 unless otherwise stated. Anti-mouse Lamin B1 (12586), STAT1 (9172), p-STAT1 (9167), JAK1 (3344), p-JAK1 (3331), TBK1 (3504), p-TBK1 (5483), STAT3 (30835), p-STAT3 (9145), FH (4567), ASS1 (70720), α-tubulin (2144), α-tubulin (3873), MAVS (4983), ATF4 (11815), p-AKT (13038), AKT (2920), p-JNK (9255), JNK (9252), p-ERK1/2 (9101), ERK1/2 (4695), p-p38 (4511), p-38 (9212), TRAF3 (4729), p-p65 (3033) and GAPDH (2118) antibodies were purchased from Cell Signaling. Anti-goat IL-1β (AF-401-NA) was purchased from R&D. Anti-2SC antibody was kindly provided by Dr. Norma Frizzell (University of South Carolina, US). Anti-mouse β-actin antibody (1/5000) (A5316) was purchased from Sigma Aldrich. Horseradish peroxidase (HRP)-conjugated anti-mouse (115-035-003), anti-goat (705-035-003) and anti-rabbit (111-035-003) immunoglobulin G (IgG) antibodies (all 1/2000) were purchased from Jackson Immunoresearch. Anti-mouse CD210 (112710) and anti-mouse IgG (406601) antibodies (both 10 μg/ml) were purchased from Biolegend. Anti-dsRNA antibody (clone rJ2, 1/60) was purchased from Merck (MABE-1134). Alexa Fluor 488 goat anti-mouse IgG1 antibody (A21121) was purchased from Invitrogen. Details of antibody validation are given in Table S1.

RT-qPCR

RNA extraction from cells was carried out using a Purelink™ RNA kit (Invitrogen) according to the manufacturer's instructions. BMDMs were treated as required, and

following treatment were instantly lysed in 350 µl RNA lysis buffer. Isolated RNA was quantified using a NanoDrop 2000 spectrophotometer, and RNA concentration was normalised to the lowest concentration across all samples with RNAse-free water. If necessary, samples were DNAse-treated after quantification using DNAse I (Thermo Fisher) according to the manufacturer's instructions. Isolated RNA samples were normalised and converted into cDNA using the High-Capacity cDNA Reverse Transcription Kit (Thermo Fisher) according to manufacturer's instructions. 10 µl of RNA (at a maximum concentration of 100 ng/µl) was added to 10 µl of reverse transcription master mix to complete the reaction mixture. Real-time quantitative PCR was performed on the cDNA generated in the previous step, using primers designed in-house and ordered from Eurofins Genomics, as detailed in Table S2**.** The reaction was performed in a 96-well qPCR plate by a 7500 Fast Real-Time PCR machine (Thermo Fisher). Relative expression ($2^{-\Delta\Delta CT}$) was calculated from the C_T values for each sample and gene of interest.

RNA Interference (RNAi)

Pre-designed silencer select siRNAs for *Cgas* (s103166), *Tmem173* (s91058), *Tlr3* (s100579), *Tlr9* (s96268), *Asl* (s99640), *Tlr7* (s100720), *Ddx58* (s106376), *Ifih1* (s89787), *Nrf2* (s70522), *Atf4* (s62689) and negative control (4390843) were ordered from Thermo Fisher**.** siRNA sequences are given in Table S2. Cells were transfected with 50 nM siRNA using 5 µl lipofectamine RNAiMAX according to manufacturer's instructions (Thermo Fisher)**.** Cells were transfected in medium without serum and antibiotics which was replaced with complete medium 8 hours later. Cells were subsequently left for at least a further 12 hours prior to treatment**.**

Immunofluorescence

Cells were plated on 20 mm cover slips in 12-well plates. Cells were treated as required and Mitotracker Red CMXRos (100 nM, Thermo Fisher), was added to medium 30 mins prior to end of cell treatments. After 30 min incubation, cells were washed three times with warm PBS. Cells were subsequently fixed for 10 mins with 4% paraformaldehyde/PBS at 37^{o}C. Cells were washed three times with PBS and permeabilized for 1 hour in block solution (1% BSA, 22.52 mg/ml glycine, 0.1% tween 20 in PBS). Anti-dsRNA antibody (Merck) was diluted 1/60 in block solution and incubated with cells overnight at room temperature. Cells were washed three times

with PBS for 5 mins/wash. A mix containing AF488-conjugated goat anti-mouse IgG1 antibody (1/1000) and DAPI (1/1000, Thermo Fisher) was subsequently added to cells for 90 mins at room temperature in the dark. Cells were subsequently washed three times with PBS for 5 mins/wash. Cover slips were mounted onto microscope slides using 10-20 µl ProLong Gold antifade reagent (Thermo Fisher). Slides were imaged using a Leica SP8 scanning confocal microscope using 20.0× objective. Images were analysed using the LAS X Life Science Microscope Software Platform (Leica). The same microscope instrument settings were used for all samples and all images were analysed using the same settings. Scale bars = 20 µm. Quantification of dsRNA or Mitotracker Red CMXRos signal intensity was performed using the measure function in ImageJ 1.53t (NIH). Mean signal intensity was calculated for individual cells in single colour images and displayed relative to signal intensity of control cells.

Flow Cytometry

Cells were plated in 12-well plates and treated as desired. CellROX Green (5 µM, Thermo Fisher) or TMRM (20 nM, Thermo Fisher) was added to cells 30 mins prior to end of cell treatments. Cells were washed once in PBS and scraped into 200 µl FACS buffer (2 mM EDTA, 0.5% FCS in PBS). Acquisition of samples was performed on a BD Accuri C6 flow cytometer. The gating strategy used for all flow cytometry experiments consisted of debris exclusion by FSC-A vs SSC-A analysis and subsequent doublet exclusion by FSC-A vs FSC-H analysis. A sample gating strategy is provided in Supplementary Fig. 2. 10,000 cells was acquired per condition. Mean fluorescence intensity (MFI) was calculated for all cells in each condition using FlowJo v10.

Liquid-Chromatography-Mass Spectrometry (LC-MS)

Steady-State Metabolomics

BMDMs (3 independent mice) were plated at 0.5 x 10^6 cells/well in 12-well plates in technical triplicate per condition, treated as indicated, snap frozen and stored at -80°C. For metabolomics on cytosolic fraction, BMDMs were plated at 10 x 10^6 cells/10 cm dish and rapid fractionation was performed as previously reported[16]. Metabolite extraction solution (MES) (methanol/acetonitrile/water, 50:30:20 v/v/v) was added (0.5 mL per 1 x 10^6 cells) and samples were incubated for 15 min on dry ice. The resulting

suspension was transferred to ice-cold microcentrifuge tubes. Samples were agitated for 20 min at 4°C in a thermomixer and then incubated at -20°C for 1 h. Samples were centrifuged at maximum speed for 10 min at 4°C. The supernatant was transferred into a new tube and centrifuged again at maximum speed for 10 min at 4°C. The supernatant was transferred to autosampler vials and stored at −80°C prior to analysis by LC-MS.

HILIC chromatographic separation of metabolites was achieved using a Millipore Sequant ZIC-pHILIC analytical column (5 µm, 2.1 × 150 mm) equipped with a 2.1 × 20 mm guard column (both 5 mm particle size) with a binary solvent system. Solvent A was 20 mM ammonium carbonate, 0.05% ammonium hydroxide; Solvent B was acetonitrile. The column oven and autosampler tray were held at 40°C and 4°C, respectively. The chromatographic gradient was run at a flow rate of 0.200 mL/min as follows: 0–2 min: 80% B; 2-17 min: linear gradient from 80% B to 20% B; 17-17.1 min: linear gradient from 20% B to 80% B; 17.1-22.5 min: hold at 80% B. Samples were randomized and analysed with LC–MS in a blinded manner and the injection volume was 5 µl. Pooled samples were generated from an equal mixture of all individual samples and analysed interspersed at regular intervals within sample sequence as a quality control. Metabolites were measured with a Thermo Scientific Q Exactive Hybrid Quadrupole-Orbitrap Mass spectrometer (HRMS) coupled to a Dionex Ultimate 3000 UHPLC or with Vanquish Horizon UHPLC coupled to an Orbitrap Exploris 240 mass spectrometer (both Thermo Fisher Scientific) via a heated electrospray ionization source.

For Thermo Scientific Q Exactive Hybrid Quadrupole-Orbitrap Mass spectrometer (HRMS) coupled to a Dionex Ultimate 3000 UHPLC, the mass spectrometer was operated in full-scan, polarity-switching mode, with the spray voltage set to +4.5 kV/-3.5 kV, the heated capillary held at 280°C and the heated electrospray ionization probe held at 320°C. The sheath gas flow was set to 40 units, the auxiliary gas flow was set to 15 units, and the sweep gas flow was set to 0 unit. HRMS data acquisition was performed in a range of m/z = 70–900, with the resolution set at 70,000, the AGC target at 1×10^6, and the maximum injection time (Max IT) at 120 ms. Metabolite identities were confirmed using two parameters: (1) precursor ion m/z was matched within 5 ppm of theoretical mass predicted by the chemical formula; (2) the retention

time of metabolites was within 5% of the retention time of a purified standard run with the same chromatographic method. Chromatogram review and peak area integration were performed using the Thermo Fisher software XCalibur Qual Browser, XCalibur Quan Browser software and Tracefinder 5.0 and the peak area for each detected metabolite was normalized against the total ion count (TIC) of that sample to correct any variations introduced from sample handling through instrument analysis. Absolute quantification of 2SC was performed by interpolation of the corresponding standard curve obtained from serial dilutions of commercially available standards (Sigma Aldrich) running with the same batch of samples.

For the Orbitrap Exploris 240 mass spectrometer, MS1 scans, mass range was set to *m/z*=70-900, AGC target set to standard and maximum injection time (IT) set to auto. Data acquisition for experimental samples used full scan mode with polarity switching at an Orbitrap resolution of 120000. Data acquisition for untargeted metabolite identification was performed using the AcquireX Deep Scan workflow, an iterative data-dependent acquisition (DDA) strategy using multiple injections of the pooled sample. In brief, sample was first injected in full scan-only mode in single polarity to create an automated inclusion list. MS2 acquisition was then carried out in triplicate, where ions on the inclusion list were prioritized for fragmentation in each run, after which both the exclusion and inclusion lists were updated in a manner where fragmented ions from the inclusion list were moved to exclusion list for the next run. DDA full scan-ddMS2 method for AcquireX workflow used the following parameters: full scan resolution was set to 60000, fragmentation resolution to 30000, fragmentation intensity threshold to 5.0e3. Dynamic exclusion was enabled after 1 time and exclusion duration was 10s. Mass tolerance was set to 5ppm. Isolation window was set to 1.2 *m/z*. Normalized HCD collision energies were set to stepped mode with values at 30, 50, 150. Fragmentation scan range was set to auto, AGC target at standard and max IT at auto. Xcalibur AcquireX method modification was on. Mild trapping was enabled.

Metabolite identification was performed in the Compound Discoverer software (v 3.2, Thermo Fisher Scientific). Metabolites were annotated at the MS2 level using both an in-house mzVault spectral database curated from 1051 authentic compound standards and the online spectral library mzCloud. The precursor mass tolerance was set to 5 ppm and fragment mass tolerance set to 10 ppm. Only metabolites with

mzVault or mzCloud best match score above 50% and 75%, respectively, and RT tolerance within 0.5 min to that of a purified standard run with the same chromatographic method were exported to generate a list including compound names, molecular formula and RT. The curated list was then used for further processing in the Tracefinder software (v 5.0, Thermo Fisher Scientific), where extracted ion chromatographs for all compounds were examined and manually integrated if necessary. False positive, noise or chromatographically unresolved compounds were removed. The peak area for each detected metabolite was then normalized against the total ion count (TIC) of that sample to correct any variations introduced from sample handling through instrument analysis. The normalized areas were used as variables for further statistical data analysis. Statistical analysis was performed using MetaboAnalyst 5.0[66].

Stable isotope-assisted tracing

BMDMs (3 independent mice) were plated at 0.5 x 10^6 cells/well in 12-well plates in technical triplicate per condition, treated as indicated in glutamine-free DMEM supplemented with U-^{13}C-glutamine or $^{15}N_2$-glutamine, respectively. For ^{13}C- and ^{15}N-tracing analysis, the theoretical masses of ^{13}C and ^{15}N isotopes were calculated and added to a library of predicted isotopes in Tracefinder 5.0. These masses were then searched with a 5-ppm tolerance and integrated only if the peak apex showed less than 1% deviation in retention time from the [U-^{12}C or ^{14}N] monoisotopic mass in the same chromatogram. The raw data obtained for each isotopologue were corrected for natural isotope abundances using the AccuCor algorithm (https://github.com/lparsons/accucor) before further statistical analysis.

EtBr Treatment

BMDMs were plated in the presence or absence of ultrapure ethidium bromide (100 ng/ml) and incubated for a further 6 days prior to treatment. Depletion of mtDNA was determined by genomic DNA isolation followed by qPCR using primers specific for areas of mitochondrial DNA (D-loop) and areas of mtDNA that are not inserted into nuclear DNA (Non-NUMT).

c-Fos Activity Assay

BMDMs from 3 mice were plated in 10 cm dishes at $0.5x10^6$ cells/mL and left overnight. Cells were pre-treated with FHIN1 or DMF (3 h) prior to LPS stimulation (4 h). Upon harvesting, nuclear extracts were isolated using a Nuclear Extraction Kit (ab113474) purchased from Abcam. Nuclear extracts were quantified via BCA assay and standardised. c-Fos relative activity was then quantified using the AP1 transcription factor assay purchased from Abcam (Ab207196) according to the manufacturers protocol.

Fumarate Assay

Analysis of fumarate levels were assessed using a fumarate colorimetric assay kit (Sigma MAK060) that uses an enzyme assay, which results in a colorimetric (450 nm) product proportional to the fumarate present, as per manufacturer's instructions.

Nitrite Measurement

The Griess Reagent System (Promega G2930) was used according to manufacturer's instructions.

RNA Sequencing

BMDMs (3 independent mice) were treated as indicated and RNA was extracted as previously detailed. mRNA was extracted from total RNA using poly-T-oligo-attached magnetic beads. After fragmentation, the first strand cDNA was synthesized using random hexamer primers, followed by the second strand cDNA synthesis. The library was checked with Qubit and real-time PCR for quantification and bioanalyzer for size distribution detection. Quantified libraries were pooled and sequenced on the NovaSeq 6000 S4 (Illumina). Differential expression analysis of two conditions/groups was performed using counted reads and the DESeq2 R package[67]. Pathway enrichment analyses were performed as indicated in quantification and statistical analysis.

Proteomic Analysis

Sample Preparation

BMDMs (from 5 independent mice) were plated onto 10-cm dishes and treated as indicated. At the experimental endpoint, cells were washed with PBS on ice and centrifuged at 1500 rpm for 5 mins at 4°C and frozen at -80°C. Cell pellets were lysed,

reduced and alkylated in 50 µl of 6M Gu-HCl, 200 mM Tris-HCl pH 8.5, 10 mM TCEP, 15 mM Chloroacetamide by probe sonication and heating to 95ºC for 5 min. Protein concentration was measured by a Bradford assay and initially digested with LysC (Wako) with an enzyme to substrate ratio of 1/200 for 4 h at 37 ºC. Subsequently, the samples were diluted tenfold with water and digested with porcine trypsin (Promega) at 37ºC overnight. Samples were acidified to 1% TFA, cleared by centrifugation (16,000 g at RT) and approximately 20 µg of the sample was desalted using a Stage-tip. Eluted peptides were lyophilized, resuspended in 0.1% TFA/water and the peptide concentration was measured by A280 on a nanodrop instrument (Thermo). The sample was diluted to 2 µg/ 5 µl for subsequent analysis.

MS Analysis

The tryptic peptides were analysed on a Fusion Lumos mass spectrometer connected to an Ultimate Ultra3000 chromatography system (both Thermo Scientific) incorporating an autosampler. 2 µg of de-salted peptides were loaded onto a 50 cm emitter packed with 1.9 µm ReproSil-Pur 200 C18-AQ (Dr Maisch, Germany) using a RSLC-nano uHPLC systems connected to a Fusion Lumos mass spectrometer (both Thermo, UK). Peptides were separated by a 140 min linear gradient from 5% to 30% acetonitrile, 0.5% acetic acid. The mass spectrometer was operated in DIA mode, acquiring a MS 350-1650 Da at 120k resolution followed by MS/MS on 45 windows with 0.5 Da overlap (200-2000 Da) at 30k with a NCE setting of 27.

Data Analysis

Raw files were analysed and quantified by searching against the Uniprot *Mus Musculus* database using DIA-NN 1.8 (https://github.com/vdemichev/DiaNN). Library-free search was selected, and the precursor ion spectra were generated from the FASTA file using the deep learning option. Default settings were used throughout apart from using “Robust LC (high precision)”. In brief, Carbamidomethylation was specified as fixed modification while acetylation of protein N-termini was specified as variable. Peptide length was set to minimum 7 amino acids, precursor FDR was set to 1%. Subsequently, missing values were replaced by a normal distribution (1.8 π shifted with a distribution of 0.3 π) to allow the following statistical analysis. Protein-wise linear models combined with empirical Bayes statistics are used for the differential

expression analyses. We use the Bioconductor package limma to carry out the analysis using the information provided in the experimental design table.

Digitonin Fractionation

BMDMs were plated at 0.5 x 10^6 cells/well and treated as desired. After treatment, cells were washed once with room temperature PBS, before being scraped on ice into ice cold PBS and pelleted at 500 x g for 5 mins at 4ºC. Supernatant was removed and discarded, and the pellet was resuspended in 400 µl extraction buffer (150 mM NaCl, 50 mM HEPES pH 7.4, 25 µg/ml digitonin). Samples were then placed in a rotating mixer at 4ºC for 10 mins before centrifugation at 2000 x g at 4ºC for 5 mins. The resulting supernatant constituted the cytosolic fraction, from which RNA and DNA were isolated using an AllPrep DNA/RNA Mini Kit (Qiagen). Alternatively, the cytosolic fraction was concentrated using Strataclean Resin (Agilent) and analysed by western blot. The pellet constituted a fraction containing membrane-bound organelles which was lysed in RNA lysis buffer for RNA isolation or lysed in western blot lysis buffer for analysis by western blot. To determine the presence of mtRNA and mtDNA in the cytosol, qPCR was performed using primers specific for mitochondrial D-loop on cDNA which had been reverse-transcribed from RNA isolated from the cytosolic fraction (mtRNA) and on DNA isolated from the cytosolic fraction (mtDNA). In both cases, values were normalised using a housekeeping control gene (β-actin) amplified in cDNA which had been reverse-transcribed from RNA isolated from the membrane-bound fraction.

MAVS Oligomerisation

BMDMs were plated at 1 x 10^6 cells/well in technical triplicate and treated as desired. After treatment, cells were washed twice with 200 µl cold PBS before being lysed in crosslinking lysis buffer (50 mM HEPES, 0.5% triton X-100, 1X protease inhibitor cocktail). Samples were placed on ice for 15 mins. Lysates were centrifuged for 15 mins at 6000 x g at 4ºC and the supernatant was removed and frozen down as the 'soluble fraction.' 20 µl of the soluble fraction was mixed with 5 µl of sample lysis buffer (0.125 M Tris pH 6.8, 10% glycerol, 0.02% SDS, 5% DTT) and run on a 10% gel. The insoluble pellet was resuspended in HEPES (50 mM) and washed 3 times by centrifuging at 6000 x g at 4ºC and removing the supernatant each time. After the final wash, the pellet was resuspended in 500 µl crosslinking buffer (50 mM HEPES, 150

mM NaCl) and disuccinimidyl suberate (DSS, Thermo Fisher, made up in anhydrous DMSO) was added to the final concentration of 2 mM. Immediately following the addition of DSS, the sample was inverted several times and incubated for 45 mins at 37ºC. The sample was then centrifuged for 15 mins at 6000 x g at 4ºC, before the supernatant was removed and the pellet was resuspended in 30 µl sample lysis buffer. The resuspended 'insoluble fraction' was subsequently boiled for 5 mins at 95ºC before being run on a gel.

Seahorse XF Glycolysis Stress Test

Cells were plated at 100,000 cells/well in 100 µl and were left overnight to adhere. Protocol was carried out according to manufacturer's instructions (Agilent). In brief, cells were treated as required, after which medium was replaced with Seahorse medium containing glutamine (2 mM). Cells were then placed in a CO_2-free incubator for 1 hour. Glycolysis stress test was subsequently performed using a Seahorse XFe96 Analyzer (Agilent) with the following injections:

A- Glucose (10 mM)
B- Oligomycin (1 µM)
C- 2-DG (50 mM)

Analysis was performed using Seahorse Wave Software (Agilent). Data shown are representative experiments containing at least 3 pooled biological replicates.

Seahorse XF Mito Stress Test

Cells were plated at 100,000 cells/well in 100 µl and were left overnight to adhere. Protocol was carried out according to manufacturer's instructions (Agilent). In brief, cells were treated as required, after which medium was replaced with Seahorse medium containing glutamine (2 mM), glucose (10 mM) and pyruvate (1 mM). Cells were then placed in a CO_2-free incubator for 1 hour. Mito stress test was subsequently performed using a Seahorse XFe96 Analyzer (Agilent) with the following injections:

A- Oligomycin (1 µM)
B- FCCP (1 µM)
C- Rotenone (500 nM)

Analysis was performed using Seahorse Wave Software (Agilent). Data shown are representative experiments containing at least 3 pooled biological replicates.

LPS-induced Inflammation Model

6-week-old male mice were used, and littermates were randomly assigned to experimental groups. Compounds were resuspended in 10% DMSO followed by 90% cyclodextrin/PBS (20% w/v). Mice were injected intraperitoneally with vehicle, FHIN1 or DMF (both 50 mg/kg) at a volume of 200 µl per injection. 1 hour later, mice were injected intraperitoneally with PBS or LPS from *E.coli* (2.5 mg/kg, Sigma) at a volume of 100 µl per injection. 2 hours later, mice were euthanised and blood was harvested retro-orbitally. Blood was allowed to clot for 30 mins at room temperature before it was centrifuged at 5000 x g for 10 mins at 4ºC. The serum was removed and IFN-β concentration was determined by ELISA.

Western Blotting

Supernatant was removed from cells following stimulation and lysates were harvested in 30-50 µl lysis buffer (0.125 M Tris pH 6.8, 10% glycerol, 0.02% SDS, 5% DTT) Lysates were subsequently heated to 95ºC for 5 mins to denature proteins. SDS-PAGE was used to resolve proteins by molecular weight. Samples were boiled at 95ºC for 5 mins prior to loading into a 5% stacking gel. The percentage resolving gel depended on the molecular weight of the given protein. The Bio-Rad gel running system was used to resolve proteins and the Bio-Rad wet transfer system was used for the electrophoretic transfer of proteins onto PVDF membrane. Following transfer, the membrane was incubated in milk powder (5% in TBST) for 1 hr and subsequently incubated in primary antibody rolling overnight at 4ºC. Primary antibodies targeting phospho-proteins were diluted in BSA (5% in TBST) as opposed to milk. The membrane was incubated for 1 hr with secondary antibody (diluted in 5% milk powder) at room temperature. Prior to visualisation, the membrane was immersed in WesternBright ECL Spray (Advansta). Protein visualisation took place on a ChemiDoc MPTM Imaging System (Bio-Rad), and both chemiluminescent and white light images were taken. Images were analysed using Image Lab 6.0.1 (Bio-Rad).

ELISA

DuoSet ELISA kits for IL-1β, TNFα, IL-6, IL-10, and GDF15 were purchased from R&D Systems and were carried out according to the manufacturer's instructions with appropriately diluted cell supernatants added to each plate in duplicate or triplicate. IFN-β was determined using DuoSet ELISA kit from R&D Systems or Abcam

(ab252363). Quantikine ELISA kit for IFN-β (R&D Systems) was used for determination of IFN-β concentration in serum samples and from human cells, and these were also carried out according to the manufacturer's instructions. Absorbance at 450 nm was quantified using a FLUOstar Optima plate reader. Corrected absorbance values were calculated by subtracting the background absorbance, and cytokine concentrations were subsequently obtained by extrapolation from a standard curve plotted on GraphPad Prism 9.2.0.

Quantification and Statistical Analyses

Details of all statistical analyses performed can be found in the figure legends. Data were expressed as mean ± standard error of the mean (SEM) unless stated otherwise. Representative western blots are shown. For metabolomics data, MetaboAnalyst 5.0[66] was used to analyse, perform statistics, and visualise the results. Autoscaling of features (metabolites) was used for heatmap generation. One-way ANOVA corrected for multiple comparisons by the Tukey statistical test was used and a p.adjusted < 0.05 was set as the cut-off. For proteomics data, protein signal intensity was converted to a $\log_2$ scale and biological replicates were grouped by experimental condition. Protein-wise linear models combined with empirical Bayes statistics were used for the differential expression analyses. The Bioconductor package limma was used to carry out the analysis using an R based online tool[68]. Data were visualised using a heatmap with autoscaled features (genes) and a Volcano plot, which shows the $\log_2$ fold change on the x axis and the $-\log_{10}$ adjusted p value on the y axis. The proteomics cut-offs for analysis were a $\log_2$FC of 0.5 and a false discovery rate (FDR) < 0.05, determined using t statistics. RNA seq cut-offs were set to $\log_2$FC of 1 and an FDR < 0.05. Overrepresentation analysis (ORA) of significant changes were assessed using Enrichr[4] and the Bioconductor package clusterProfiler 4.0 in R (version 3.6.1). Further information on this visualisation method is available[69]. Emapplots were generated using enrichplot package in R (version 3.6.1). GSEA analysis of RNAseq was performed using the Broad Institutes GSEA 4.1.0[70]. Graphpad Prism 9.2.0 was used to calculate statistics in bar plots using appropriate statistical tests depending on the data including one-way ANOVA, two-tailed unpaired t test and multiple t tests. Adjusted p values were assessed using appropriate correction methods, such as Tukey, Kruskal-Wallis, and Holm-Sidak tests. Sample sizes were determined based on previous experiments using similar methodologies. All depicted data points are

biological replicates taken from distinct samples, unless stated otherwise. Each figure consists of a minimum of 3 independent experiments from multiple biological replicates, unless stated otherwise. For *in vivo* studies, mice were randomly assigned to treatment groups. For metabolomics, proteomics and RNA sequencing analyses, samples were processed in random order and experimenters were blinded to experimental conditions.

Data Availability

Proteomics data from Fig. 1d were previously deposited to the ProteomeXchange Consortium via the PRIDE partner repository with the dataset identifier PXD029155[11]. All other proteomics, RNA sequencing data and metabolomics data have been deposited to Dryad (doi:10.5061/dryad.6wwpzgn28). All original gel images are provided in the source data file. All other source data are available from the corresponding author(s) upon request.

References (methods)

66. Pang, Z. *et al.* MetaboAnalyst 5.0: narrowing the gap between raw spectra and functional insights. *Nucleic Acids Res* **49**, W388-W396, doi:10.1093/nar/gkab382 (2021).
67. Anders, S. & Huber, W. Differential expression analysis for sequence count data. *Genome Biol* **11**, R106, doi:10.1186/gb-2010-11-10-r106 (2010).
68. Shah, A. D., Goode, R. J. A., Huang, C., Powell, D. R. & Schittenhelm, R. B. LFQ-Analyst: An Easy-To-Use Interactive Web Platform To Analyze and Visualize Label-Free Proteomics Data Preprocessed with MaxQuant. *J Proteome Res* **19**, 204-211, doi:10.1021/acs.jproteome.9b00496 (2020).
69. Kuleshov, M. V. *et al.* Enrichr: a comprehensive gene set enrichment analysis web server 2016 update. *Nucleic Acids Res* **44**, W90-97, doi:10.1093/nar/gkw377 (2016).
70. Subramanian, A. *et al.* Gene set enrichment analysis: a knowledge-based approach for interpreting genome-wide expression profiles. *Proc Natl Acad Sci U S A* **102**, 15545-15550, doi:10.1073/pnas.0506580102 (2005).

Acknowledgements

We would like to thank the O'Neill lab for helpful discussions and Novogene for assistance with RNA sequencing. We would like to thank Dr Barry Moran and Dr Gavin McManus (both Trinity College Dublin) for assistance with flow cytometry and confocal microscopy respectively. We would like to thank Dr Ashish Dhir (University of Edinburgh) for helpful discussions. We would like to thank Ms. Anna Capps for assistance with anti-2SC immunoblotting. L.A.O'N. was funded by European Research Council (Metabinnate 834370) and Science Foundation Ireland (20/SPP/3685). A.V.K was funded by Wellcome Trust (Multiuser Equipment Grant, 208402/Z/17/Z). N.F. was funded by NIH (R01NS1268). C.Je was funded by NIH (R01AI164504), the Office of the Assistant Secretary of Defense for Health Affairs through the Department of Defense Lupus Research Program (LRP), (W81XWH-18-1-0709), and Cedars-Sinai Precision Health RFP 2020. Schematic figures were created using BioRender.com

Author contributions

A.H., C.G.P., D.G.R. and L.A.J.O'N. conceptualised the project; A.H., C.G.P. and D.G.R. were lead experimentalists, provided intellectual input, designed all experiments, analysed and visualised the data and co-wrote the paper with input from all authors. E.A.D performed *in vivo* experiments. E.N.M., L.H., G.D.L.S., M.I., D.J.W., S.V. and C.Je. generated data from SLE patients. J.E.T.K. assisted with immunofluorescence experiments. C.F., M.Ya., A.S.H.C. and E.P. assisted with metabolomics. A.B.C. and A.V.K. assisted with proteomics. A.F.M., M.Yi., T.A.J.R., A.M.C. and H.A.P. performed *in vitro* experiments. C.F. and V.Z. provided inducible *Fh1*$^{+/fl}$ and *Fh1*$^{fl/fl}$ mouse tissue. N.F. verified protein succination with 2SC antibody on provided macrophage lysates. C.Jo. provided *Mavs*$^{-/-}$ mouse tissue. M.P.M. and C.F. provided intellectual input and oversaw a portion of the research programme. L.A.J.O'N. obtained funding and oversaw the research programme.

Competing interests

The authors declare no competing interests.

Materials & Correspondence

Correspondence and materials request should be addressed to A.H, D.G.R or L.A.J.O'N.

Extended Data Figure 1 – LPS stimulation drives fumarate accumulation and protein succination

a-c, Fumarate-mediated protein succination with LPS (*n* = 3) and 2SC abundance in NS and LPS-stimulated BMDMs (*n* = 5; LPS 4 h). **d**, Heatmap of metabolites linked to aspartate-argininosuccinate shunt in NS and LPS-stimulated BMDMs (*n* = 5; LPS 24 h) **e,** Metabolite abundance of aspartate-argininosuccinate shunt metabolites in LPS-stimulated BMDMs pre-treated with DMSO or AOAA (*n* = 3; LPS 4 h; aspartate (P=0.0000005)). **f,** *Asl* expression with silencing of *Asl* following LPS stimulation (*n* = 3; LPS 24 h). **g,** Fumarate levels with silencing of *Asl* following LPS stimulation (*n* = 3; LPS 24 h). **c,e-h,** Data are mean ± s.e.m. **a,** 1 representative blot of 3 shown. *n* = biological replicates. *P* values calculated using two-tailed Student's *t*-test for paired comparisons or one-way ANOVA for multiple comparisons.

Extended Data Figure 2 – LPS stimulation drives fumarate accumulation via glutamine anaplerosis and an aspartate-argininosuccinate shunt

a, Schematic diagram indicating U-^{13}C-glutamine tracing into distinct metabolic modules. **b,** U-^{13}C-glutamine tracing into glutamate, α-KG and succinate in LPS-treated BMDMs (m+4 and m+5 labelling intensity and total isotopologue fraction distribution) (*n* = 3; LPS 4 h). **c,** U-^{13}C-glutamine tracing into γ-glutamylcysteine, GSH and GSSG in LPS-treated BMDMs (m+5 labelling intensity and total isotopologue fraction distribution) (*n* = 3; LPS 4 h). **d,** U-^{13}C-glutamine tracing into aspartate, argininosuccinate, fumarate and malate in LPS-treated BMDMs (m+4 labelling intensity and total isotopologue fraction distribution) (*n* = 3; LPS 4 h). Data are mean ± s.e.m. *n* = biological replicates. *P* values calculated using two-tailed Student's t-test for paired comparisons.

Extended Data Figure 3 – LPS stimulation drives fumarate accumulation via glutamine anaplerosis and an aspartate-argininosuccinate shunt

a, Schematic diagram indicating $^{15}N_2$-glutamine tracing into distinct metabolic modules. **b,** $^{15}N_2$-glutamine tracing into glutamate and asparagine in LPS-treated BMDMs (m+1 and m+2 labelling intensity and total isotopologue fraction distribution) (*n* = 3; LPS 4 h). **c,** $^{15}N_2$-glutamine tracing into GSH and GSSG in LPS-treated BMDMs (m+1 and m+2 labelling intensity and total isotopologue fraction distribution) (*n* = 3; LPS 4 h). **d,** $^{15}N_2$-glutamine tracing into aspartate, arginine and citrulline in LPS-treated BMDMs (m+1 labelling intensity and total isotopologue fraction distribution) (*n* = 3; LPS 4 h; aspartate (P=0.000001)). Data are mean ± s.e.m. *n* = biological replicates. *P* values calculated using one-way ANOVA for multiple comparisons.

Extended Data Figure 4 – Increase in aspartate-argininosuccinate shunt metabolites in cytosol and *Irg1*$^{-/-}$ macrophages

Heatmap (min-max) of metabolites linked to mitochondrial bioenergetics and redox signalling (**a**) and the aspartate-argininosuccinate shunt (**b**) in NS and BMDMs (n = 3; LPS 24 h). **c,** Metabolite abundance of TCA cycle and aspartate-argininosuccinate shunt metabolites in WT and *Irg1*$^{-/-}$ BMDMs (n = 3; LPS 24 h; itaconate (P=0.00000000000002, succinate (P=0.00000003), fumarate (P=0.000018)). **d,** Nitrite levels in WT and *Irg1*$^{-/-}$ BMDMs (n = 3; LPS 24 h). **e,** Schematic of metabolic changes occurring during mid-phase TCA cycle rewiring in WT and *Irg1*$^{-/-}$ BMDMs. Created with BioRender.com. Data are mean ± s.e.m. n = biological replicates. P values calculated using two-tailed Student's t-test for paired comparisons or one-way ANOVA for multiple comparisons.

Extended Data Figure 5 – FH deletion increases bioenergetic stress, fumarate, and mitochondrial membrane potential

a, Bioenergetic ratios in BMDMs treated with DMSO or FHIN1 (n = 3). **b,** Fumarate and 2SC levels in BMDMs treated with DMSO or FHIN1 (n = 3). qPCR (n = 5) (**c**) and western blot (n = 2) (**d**) analysis of *Fh1* expression in *Fh1*$^{+/+}$ and *Fh1*$^{-/-}$ BMDMs (EtOH/TAM 72 h; LPS 4 h; *Fh1*$^{+/+}$ NS vs *Fh1*$^{+/+}$LPS (P=0.00000002), *Fh1*$^{+/+}$ NS vs *Fh1*$^{-/-}$ NS (P=0.00000000000002), *Fh1*$^{-/-}$ NS vs *Fh1*$^{-/-}$ LPS (P=0.0000000000014)). **e,** Bioenergetic ratios in *Fh1*$^{+/+}$ and *Fh1*$^{-/-}$ BMDMs (n = 3; EtOH/TAM 48 h). **f,** Heatmap of top 50 significantly abundant metabolites in *Fh1*$^{+/+}$ and *Fh1*$^{-/-}$ BMDMs (n = 3; LPS 4 h). **g,** Fumarate and 2SC levels in *Fh1*$^{+/+}$ and *Fh1*$^{-/-}$ BMDMs (n = 3; EtOH/TAM 72 h). **h,** Glycolysis as measured by ECAR in BMDMs pre-treated with DMSO, FHIN1 or DMF (n = 8 (DMSO/FHIN1); n = 6 (DMF); LPS 4 h). n = technical replicates from 1 experiment performed with 3 pooled biological replicates. Data are mean ± s.d. **i,** Glyceraldehyde 3- phosphate (G3P) and 2,3-phosphoglycerate (2/3-PG) levels and ratio in BMDMs pre-treated with DMSO or FHIN1 (n = 3; LPS 4 h; G3P (P=0.00004)). Immunofluorescence (**k**) and quantification (**j**) of Mitotracker red staining in BMDMs pre-treated with DMSO or FHIN1 (n = 8 (DMSO); n = 19 (FHIN1); LPS 4 h). n = technical replicates from representative experiment. Scale bar = 20 μm. Data are mean ± s.d. **a-c,e,g,i** Data are mean ± s.e.m. Representative blots or images of 2 (**d**) or 1 experiment(s) (**j**) shown. n = biological replicates unless stated otherwise. P values calculated using two-tailed Student's t-test for paired comparisons or one-way ANOVA for multiple comparisons.

Extended Data Figure 6 – FH inhibition remodels inflammatory gene expression

a, *Il10* and *Tnfa* expression in BMDMs pre-treated with DMSO, FHIN1 or DMF (n = 5 *(Il10*); n = 6 (*Tnfa*); LPS 4 h; FHIN1/*Il10* P=0.000002, DMF/*Il10* P=0.0000004)). **b**, *Il1b* expression and IL-6 release in BMDMs pre-treated with DMSO, FHIN1 or DMF (n = 6; 4 h LPS; DMF/*Il1b* (P=0.000046), DMF/IL-6 (P=0.00000002)). **c**, Enrichment map plot of shared significantly increased genes in BMDMs pre-treated with DMF or FHIN1 compared to DMSO control (n = 3; LPS 4 h). **d,** Western blot of total and phospho-AKT, JNK, ERK and p38 levels in BMDMs pre-treated with DMSO, FHIN1 or DMF (n = 2). **e,** *Jun* expression in RNA seq from BMDMs pre-treated with DMF or FHIN1 compared to DMSO control (n = 3; LPS 4 h). **f**, *Fos* expression in RNA seq from BMDMs pre-treated with DMF or FHIN1 compared to DMSO control (n = 3; LPS 4 h). **g,** Western blot of total and phospho-STAT3 levels in BMDMs pre-treated with anti-CD210 antibody (1 h) (n = 4; LPS 4 h). **h,** FH protein and gene expression levels in $Fh1^{+/+}$ and $Fh1^{+/-}$ BMDMs (n = 2; EtOH/TAM 72 h). **i,** ELISA of IL-10 and TNF-α release in BMDMs pre-treated with DMSO or AOAA (n = 3; LPS 4 h; IL-10 (P=0.000483)). **j,** Schematic depicting mild suppression of IL-10 expression during typical LPS signalling (right), and increased suppression of IL-10 following FH inhibition, leading to dysregulated TNF-α release (right). Created with BioRender.com. **a,b,e,f,h,i** Data are mean ± s.e.m. 1 representative blot of 2 (**d, h**) or 4 (**g**) shown. n = biological replicates. P values calculated using two-tailed Student's t-test for paired comparisons or one-way ANOVA for multiple comparisons.

Extended Data Figure 7 – FH inhibition triggers the NRF2 and ATF4 stress response and promotes GDF15 release

a, Heatmap of significantly differentially expressed RNA seq data in BMDMs pre-treated with FHIN1 compared to DMSO control (n = 3; LPS 4 h). Volcano plots of proteomics in BMDMs pre-treated with DMSO, FHIN1 (**b**) or DMF (**c**) (n = 5; LPS 4 h). **d,** ELISA of GDF15 in BMDMs pre-treated with DMSO or FHIN1 (n = 3; LPS 4 h). **e,** *Nrf2* expression or ATF4 protein levels after silencing of *Nrf2* or *Atf4*, respectively, in BMDMs pre-treated with DMSO or FHIN1 (n = 6; LPS 4 h). **f,** *Gdf15* expression after silencing of *Nrf2* or *Atf4* respectively in BMDMs pre-treated with DMSO or FHIN1 (n = 3, LPS 4 h; FHIN1/*Nrf2* RNAi (P=0.000048)). **d-f,** Data are mean ± s.e.m. **e,** 1 representative blot of 6 shown. n = biological replicates unless stated otherwise. P values calculated using one-way ANOVA for multiple comparisons.

Extended Data Figure 8 – IFN-β release following FH inhibition is independent of cGAS-STING

a, Heatmap (min-max) of significantly differentially expressed RNA seq data in BMDMs pre-treated with DMSO or DMF (*n* = 3; LPS 4 h). **b**, Phospho-STAT1, STAT1, phospho-JAK1 and JAK1 levels in BMDMs pre-treated with DMSO, FHIN1 or DMF (*n* = 3; LPS 4 h). **c**, *Ifnb1* expression after silencing of *Nrf2* in BMDMs pre-treated with DMSO, FHIN1 or DMF (*n* = 3, LPS 4 h). **d,** *Nrf2* expression after silencing of *Nrf2* in BMDMs pre-treated with DMSO, FHIN1 or DMF (*n* = 3, LPS 4 h; FHIN1 (P=0.0000008), DMF (P=0.0000012)). **e,** *Ifnb1* expression in BMDMs pre-treated with DMSO or FHIN1 in the presence of NAC (*n* = 3; LPS 4 h). **f**, TRAF3 levels in BMDMs pre-treated with DMSO or FHIN1 (*n* = 3; LPS 4 h). **g,** IL-1β levels in BMDMs pre-treated with DMSO, FHIN1 or DMF (*n* = 3). **h,** p-p65 levels in BMDMs pre-treated with DMSO, FHIN1 or DMF (*n* = 3). **i,** *D-loop* and *Non-NUMT* DNA fold expression in EtBr-treated BMDMs (*n* = 5; *D-loop* (P=000000000031, *Non-NUMT* (P=0.0000000012). **j,** Lamin B1 and α-tubulin in cytosolic and membrane-bound organelle fractions following digitonin fractionation (*n* = 3). **k**, IFN-β release from 2',3' cGAMP- or CpG-transfected BMDMs pre-treated (1 h) with C-178 or ODN2088 (*n* = 3 (cGAMP); *n* = 4(CpG); 3 h). **l,** *Ifnb1* expression in BMDMs pre-treated with DMSO or FHIN1 in conjunction with C-178 or ODN2088 (1 h) respectively (*n* = 3; LPS 4 h). **m,** *Cgas, Tmem173* and *Tlr9* expression with silencing of *Cgas, Tmem173* and *Tlr9* respectively in BMDMs pre-treated with DMSO or FHIN1 (*n* = 3; LPS 4 h). **n,** IFN-β release with silencing of *Cgas, Tmem173* and *Tlr9* respectively from BMDMs pre-treated with DMSO or FHIN1 (*n* = 3; LPS 4 h). **o,** *Tmem173* expression in BMDMs pre-treated with DMSO, FHIN1 or DMF (*n* = 3, LPS 4 h). **p,** *ND4, ND5* and *ND6* RNA levels in whole cell extracts of BMDMs pre-treated with DMSO or FHIN1 in the presence of IMT1 (*n* = 5; LPS 4 h; *ND5* (P=0.000052)). **q,** *ND4, ND5* and *ND6* RNA levels in cytosolic extracts of BMDMs pre-treated with DMSO or FHIN1 in the presence or absence of IMT1 (*n* = 5; LPS 4 h). **r,** IFN-β release in BMDMs pre-treated with DMSO or FHIN1 in the presence of IMT1 (*n* = 3; LPS 4 h). **c-e,i,k-r,** Data are mean ± s.e.m. **b,f-h,j,** 1 representative of 3 shown. *n* = biological replicates. *P* values calculated using two-tailed Student's t-test for paired comparisons or one-way ANOVA for multiple comparisons.

Extended Data Figure 9 – Mitochondrial membrane potential modifiers increase mtRNA and trigger IFN-β release

a, *Tlr7* expression with silencing of *Tlr7* in BMDMs pre-treated with DMSO or FHIN1 (*n* = 3; LPS 4 h). **b,** *Ddx58* and *Ifih1* expression with silencing of *Ddx58* and *Ifih1* respectively in BMDMs pre-treated with DMSO or FHIN1 (*n* = 5; LPS 4 h; DMSO/*Ddx58* (P=0.000000000002), FHIN1/*Ddx58* (P=0.000000813792), DMSO/*Ifih1* (P=0.00000009), FHIN1/*Ifih1* (P=0.00000014)). **c,** *Tlr3* expression and IFN-β release with silencing of *Tlr3* in BMDMs pre-treated with DMSO or FHIN1 (*n* = 3; LPS 4 h; DMSO/*Tlr3* (P=0.000000007), FHIN1/*Tlr3* (P=0.000013487)). **d,** TBK1 and p-TBK1 in BMDMs pre-treated with DMSO or FHIN1 (*n* = 3; LPS 4 h). **e,** *Ifnb1* expression in WT and *Mavs*$^{-/-}$ BMDMs pre-treated with DMSO or FHIN1 (*n* = 3; LPS 4 h). **f,** MFI of TMRM staining in BMDMs pre-treated with DMSO, FHIN1, oligomycin or valinomycin (n = 3, LPS 4 h). **g**, IFN-β release from BMDMs pre-treated with DMSO, FHIN1, oligomycin or valinomycin (*n* = 4; LPS 4 h; oligomycin (P=0.0000003)). **h,** MFI of TMRM staining and IFN-β release from BMDMs pre-treated with DMSO or CCCP (*n* = 4 (TMRM), *n* = 3 (IFN-β); LPS 4 h; CCCP/IFN-β (P=0.00000008). **i,** MFI of TMRM staining in BMDMs pre-treated with DMSO or MMF (n = 3, LPS 4 h). Immunofluorescence (**j**) and quantification (**k**) of dsRNA in BMDMs pre-treated with DMSO, FHIN1 or oligomycin or transfected with poly (I:C) (*n* = 8; LPS 4 h). *n* = technical replicates from representative experiment. Data are mean ± s.d. Scale bar = 20 μm. **l,** *D-loop* fold expression in DNA and RNA isolated from cytosolic fractions of digitonin-fractionated BMDMs pre-treated with DMSO or oligomycin (*n* = 4 for mtDNA, *n* = 5 for mtRNA). Immunofluorescence (**m**) and quantification (**n**) of dsRNA in BMDMs pre-treated with DMSO or valinomycin (*n* = 9 (DMSO); *n* = 6 (Valinomycin); LPS 4 h). *n* = technical replicates from representative experiment. Data are mean ± s.d. Scale bar = 20 μm. **o,** Quantification of dsRNA immunofluorescence in *Fh1*$^{+/+}$ and *Fh1*$^{-/-}$ BMDMs (*n* = 7 (*Fh1*$^{+/+}$ Control); *n* = 6 (*Fh1*$^{+/+}$ LPS); *n* = 12 (*Fh1*$^{-/-}$ Control); *n* = 10 (*Fh1*$^{-/-}$ LPS); EtOH/TAM 72 h; LPS 4 h). *n* = technical replicates from representative experiment. Data are mean ± s.d. **a-c,e-i,l** Data are mean ± s.e.m. **d,j,m,** 1 representative blot or image of 3 experiments shown. *n* = biological replicates unless stated otherwise. *P* values calculated using two-tailed Student's t-test for paired comparisons, one-way ANOVA for multiple comparisons.

Extended Data Figure 10- Prolonged LPS stimulation increases mitochondrial membrane potential and dsRNA

a, MFI of TMRM staining in BMDMs (*n* = 3). Immunofluorescence (**b**) and quantification (**c**) of dsRNA in BMDMs (*n* = 8 (0/48 h); *n* = 9 (24 h)). *n* = technical replicates from representative experiment. Data are mean ± s.d. Scale bar = 20 μm. **d,** *Ddx58* and *Ifih1* expression in BMDMs (*n* = 4; LPS 4 h; *Ddx58* (P=0.0000000010), *Ifih1* (P=0.00000012)). **e,** *Fh1* expression in IFN-β-stimulated BMDMs (*n* = 3). **a,d,e,** Data are mean ± s.e.m. **b,** 1 representative image of 3 experiments shown. *n* = biological replicates unless stated otherwise. *P* values calculated using two-tailed Student's t-test for paired comparisons, one-way ANOVA for multiple comparisons.

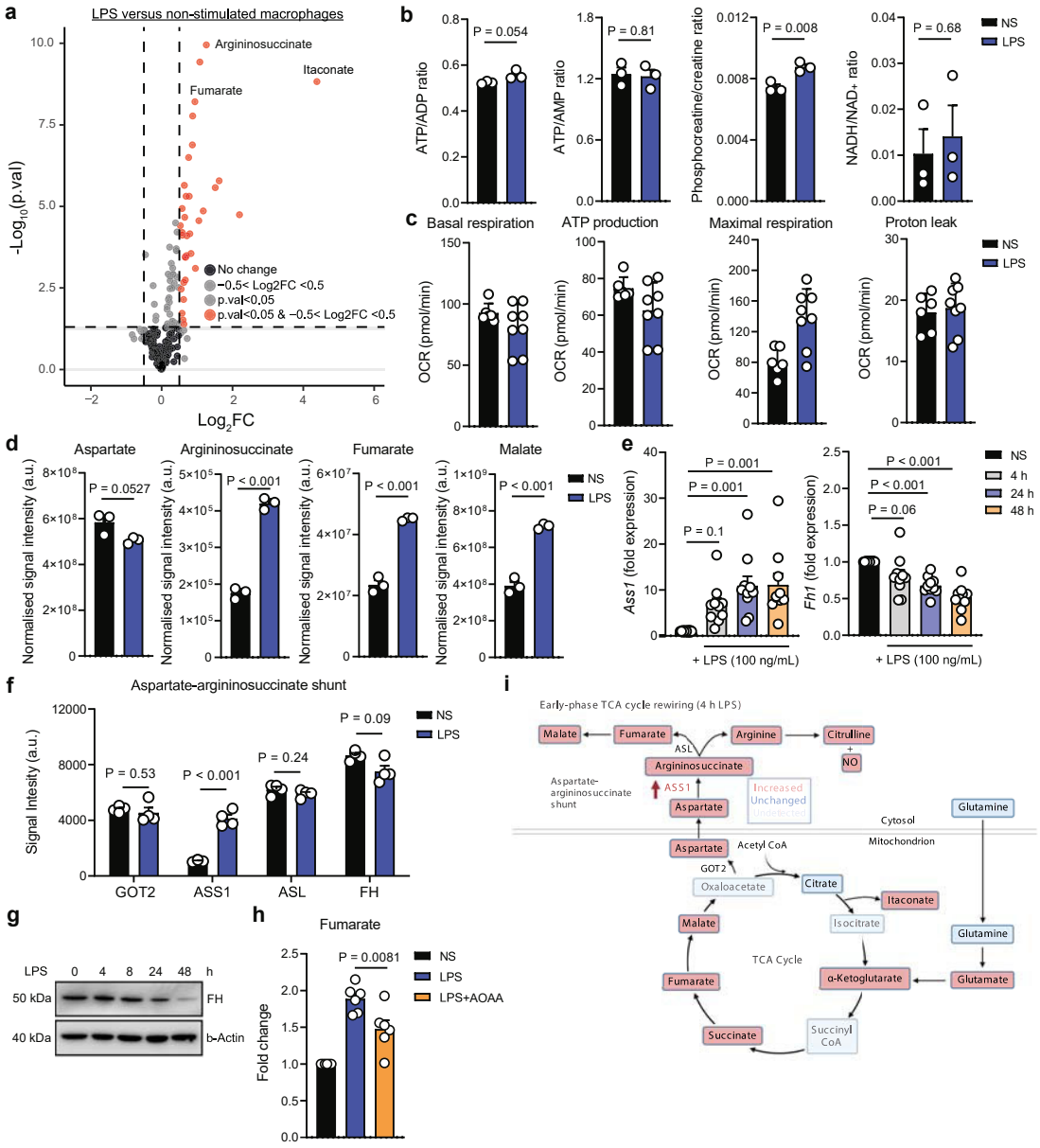
a
LPS versus non-stimulated macrophages
Argininosuccinate
Itaconate
Fumarate
No change
−0.5< Log2FC <0.5
p.val<0.05
p.val<0.05 & −0.5< Log2FC <0.5
-Log10(p.val)
Log2FC
b
ATP/ADP ratio
P = 0.054
ATP/AMP ratio
P = 0.81
Phosphocreatine/creatine ratio
P = 0.008
NADH/NAD+ ratio
P = 0.68
NS
LPS
c
Basal respiration
ATP production
Maximal respiration
Proton leak
OCR (pmol/min)
d
Aspartate
Argininosuccinate
Fumarate
Malate
Normalised signal intensity (a.u.)
P = 0.0527
P < 0.001
e
Ass1 (fold expression)
Fh1 (fold expression)
P = 0.001
P = 0.1
P < 0.001
P = 0.06
+ LPS (100 ng/mL)
4 h
24 h
48 h
f
Aspartate-argininosuccinate shunt
Signal Intesity (a.u.)
P = 0.53
P < 0.001
P = 0.24
P = 0.09
GOT2
ASS1
ASL
FH
g
LPS
0
4
8
24
48
h
50 kDa
FH
40 kDa
b-Actin
h
Fumarate
Fold change
P = 0.0081
LPS+AOAA
i
Early-phase TCA cycle rewiring (4 h LPS)
Malate
Fumarate
Arginine
Citrulline
NO
ASL
Argininosuccinate
ASS1
Aspartate
Aspartate-argininosuccinate shunt
Increased
Unchanged
Undetected
Glutamine
Cytosol
Mitochondrion
Acetyl CoA
GOT2
Oxaloacetate
Citrate
Itaconate
Isocitrate
TCA Cycle
α-Ketoglutarate
Glutamate
Succinyl CoA
Succinate

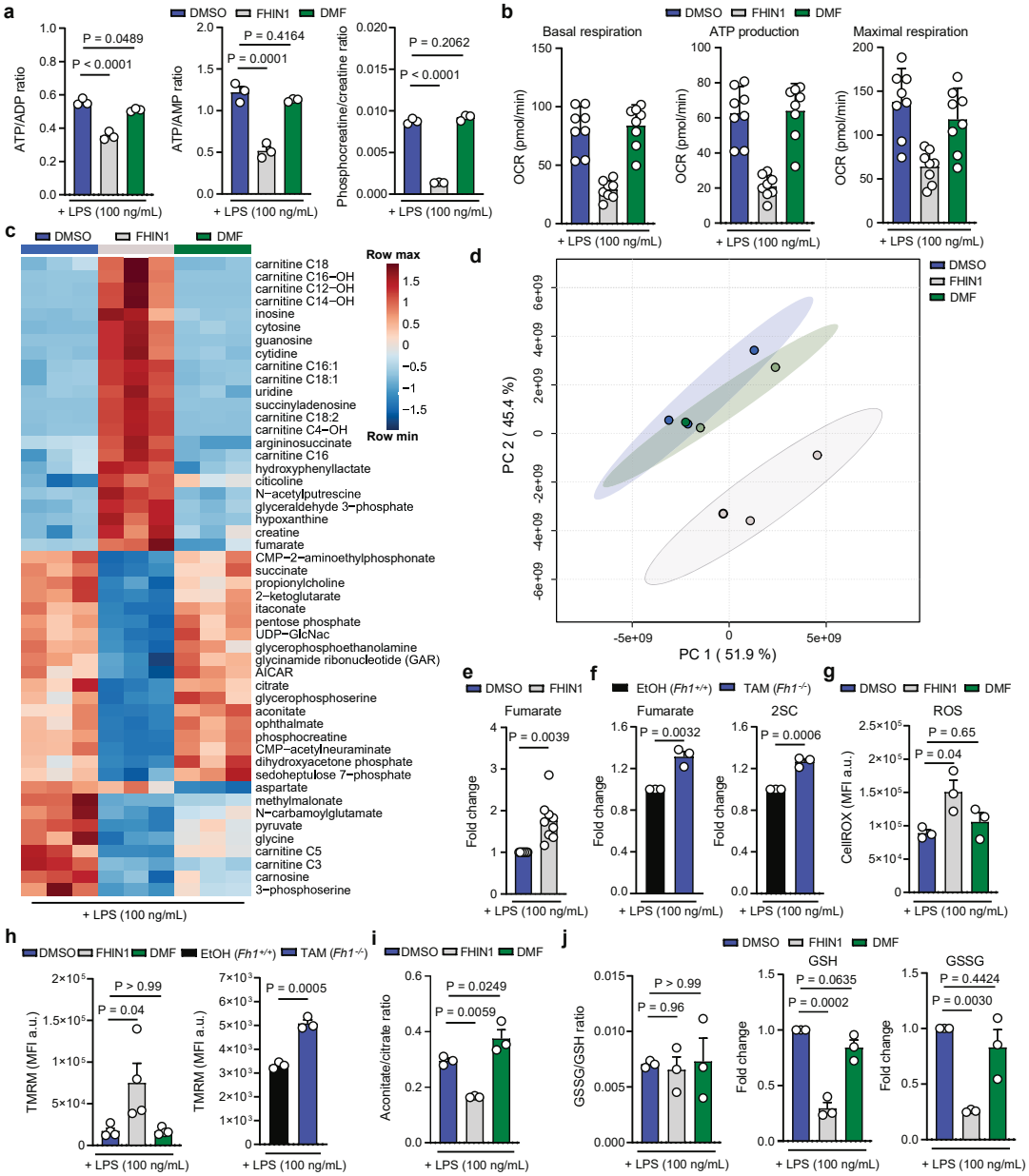
a
DMSO FHIN1 DMF
ATP/ADP ratio
P = 0.0489
P < 0.0001
ATP/AMP ratio
P = 0.4164
P = 0.0001
Phosphocreatine/creatine ratio
P = 0.2062
P < 0.0001
+ LPS (100 ng/mL)
b
Basal respiration
ATP production
Maximal respiration
OCR (pmol/min)
c
Row max
Row min
carnitine C18
carnitine C16−OH
carnitine C12−OH
carnitine C14−OH
inosine
cytosine
guanosine
cytidine
carnitine C16:1
carnitine C18:1
uridine
succinyladenosine
carnitine C18:2
carnitine C4−OH
argininosuccinate
carnitine C16
hydroxyphenyllactate
citicoline
N−acetylputrescine
glyceraldehyde 3−phosphate
hypoxanthine
creatine
fumarate
CMP−2−aminoethylphosphonate
succinate
propionylcholine
2−ketoglutarate
itaconate
pentose phosphate
UDP−GlcNac
glycerophosphoethanolamine
glycinamide ribonucleotide (GAR)
AICAR
citrate
glycerophosphoserine
aconitate
ophthalmate
phosphocreatine
CMP−acetylneuraminate
dihydroxyacetone phosphate
sedoheptulose 7−phosphate
aspartate
methylmalonate
N−carbamoylglutamate
pyruvate
glycine
carnitine C5
carnitine C3
carnosine
3−phosphoserine
d
PC 2 (45.4 %)
PC 1 (51.9 %)
e
Fumarate
Fold change
P = 0.0039
f
EtOH (Fh1+/+)
TAM (Fh1−/−)
Fumarate
P = 0.0032
2SC
P = 0.0006
g
ROS
CellROX (MFI a.u.)
P = 0.65
P = 0.04
h
TMRM (MFI a.u.)
P > 0.99
P = 0.04
P = 0.0005
i
Aconitate/citrate ratio
P = 0.0249
P = 0.0059
j
GSSG/GSH ratio
P > 0.99
P = 0.96
GSH
P = 0.0635
P = 0.0002
GSSG
P = 0.4424
P = 0.0030

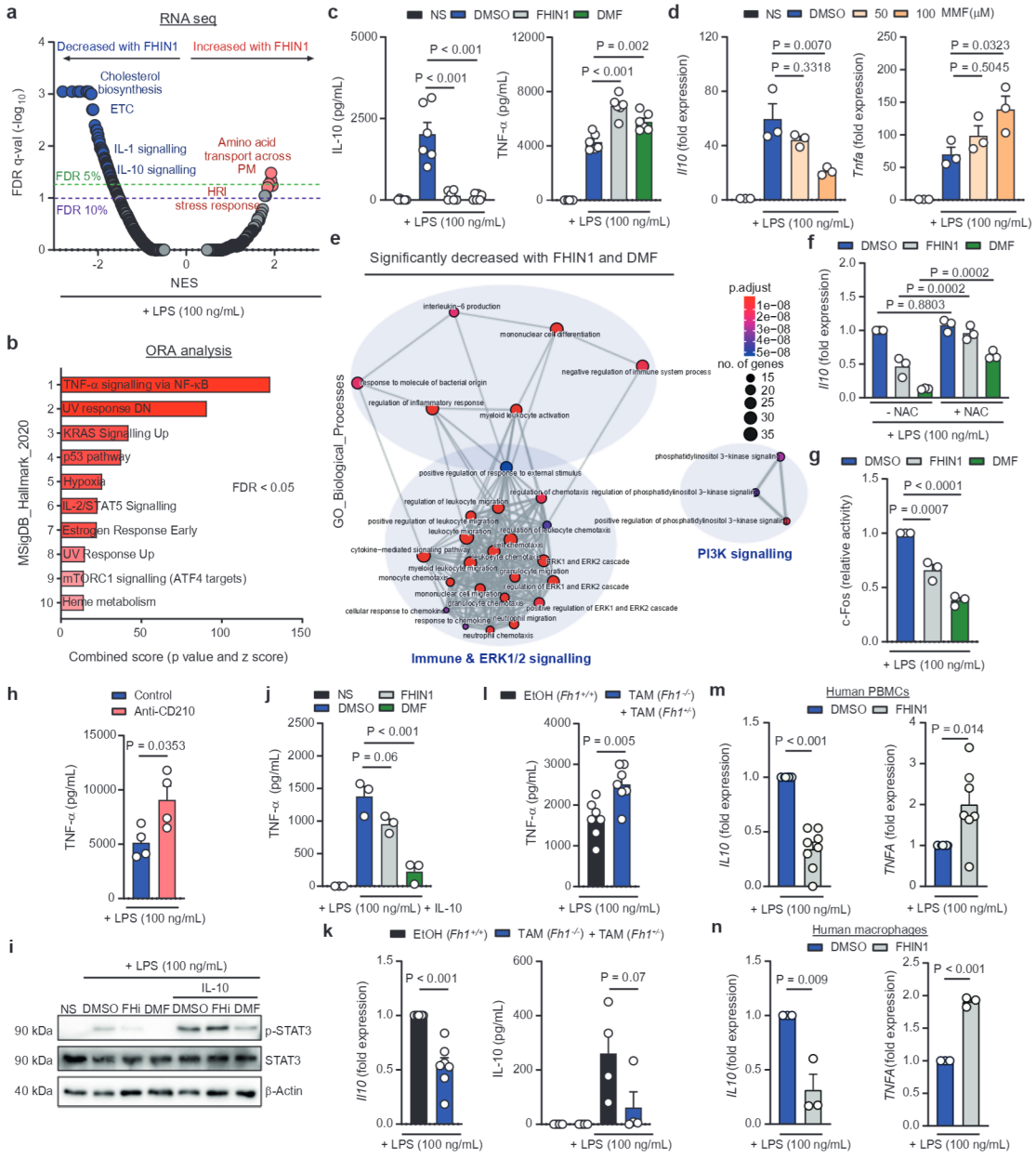
a
RNA seq
Decreased with FHIN1
Increased with FHIN1
Cholesterol biosynthesis
ETC
IL-1 signalling
IL-10 signalling
Amino acid transport across PM
HRI stress response
FDR 5%
FDR 10%
FDR q-val (-log10)
NES
+ LPS (100 ng/mL)
b
ORA analysis
MSigDB_Hallmark_2020
TNF-α signalling via NF-κB
UV response DN
KRAS Signalling Up
p53 pathway
Hypoxia
IL-2/STAT5 Signalling
Estrogen Response Early
UV Response Up
mTORC1 signalling (ATF4 targets)
Heme metabolism
FDR < 0.05
Combined score (p value and z score)
c
NS DMSO FHIN1 DMF
IL-10 (pg/mL)
TNF-α (pg/mL)
P < 0.001
P = 0.002
+ LPS (100 ng/mL)
d
NS DMSO 50 100 MMF(μM)
Il10 (fold expression)
Tnfa (fold expression)
P = 0.0070
P = 0.3318
P = 0.0323
P = 0.5045
e
Significantly decreased with FHIN1 and DMF
GO_Biological_Processes
p.adjust
no. of genes
PI3K signalling
Immune & ERK1/2 signalling
f
DMSO FHIN1 DMF
Il10 (fold expression)
P = 0.0002
P = 0.0002
P = 0.8803
- NAC
+ NAC
g
DMSO FHIN1 DMF
c-Fos (relative activity)
P < 0.0001
P = 0.0007
h
Control
Anti-CD210
TNF-α (pg/mL)
P = 0.0353
i
+ LPS (100 ng/mL)
IL-10
NS DMSO FHi DMF DMSO FHi DMF
90 kDa
p-STAT3
STAT3
40 kDa
β-Actin
j
NS DMSO FHIN1 DMF
P < 0.001
P = 0.06
+ LPS (100 ng/mL) + IL-10
l
EtOH (Fh1+/+) TAM (Fh1-/-) + TAM (Fh1+/-)
P = 0.005
m
Human PBMCs
DMSO FHIN1
IL10 (fold expression)
TNFA (fold expression)
P < 0.001
P = 0.014
k
EtOH (Fh1+/+) TAM (Fh1-/-) + TAM (Fh1+/-)
P < 0.001
P = 0.07
n
Human macrophages
DMSO FHIN1
P = 0.009
P < 0.001

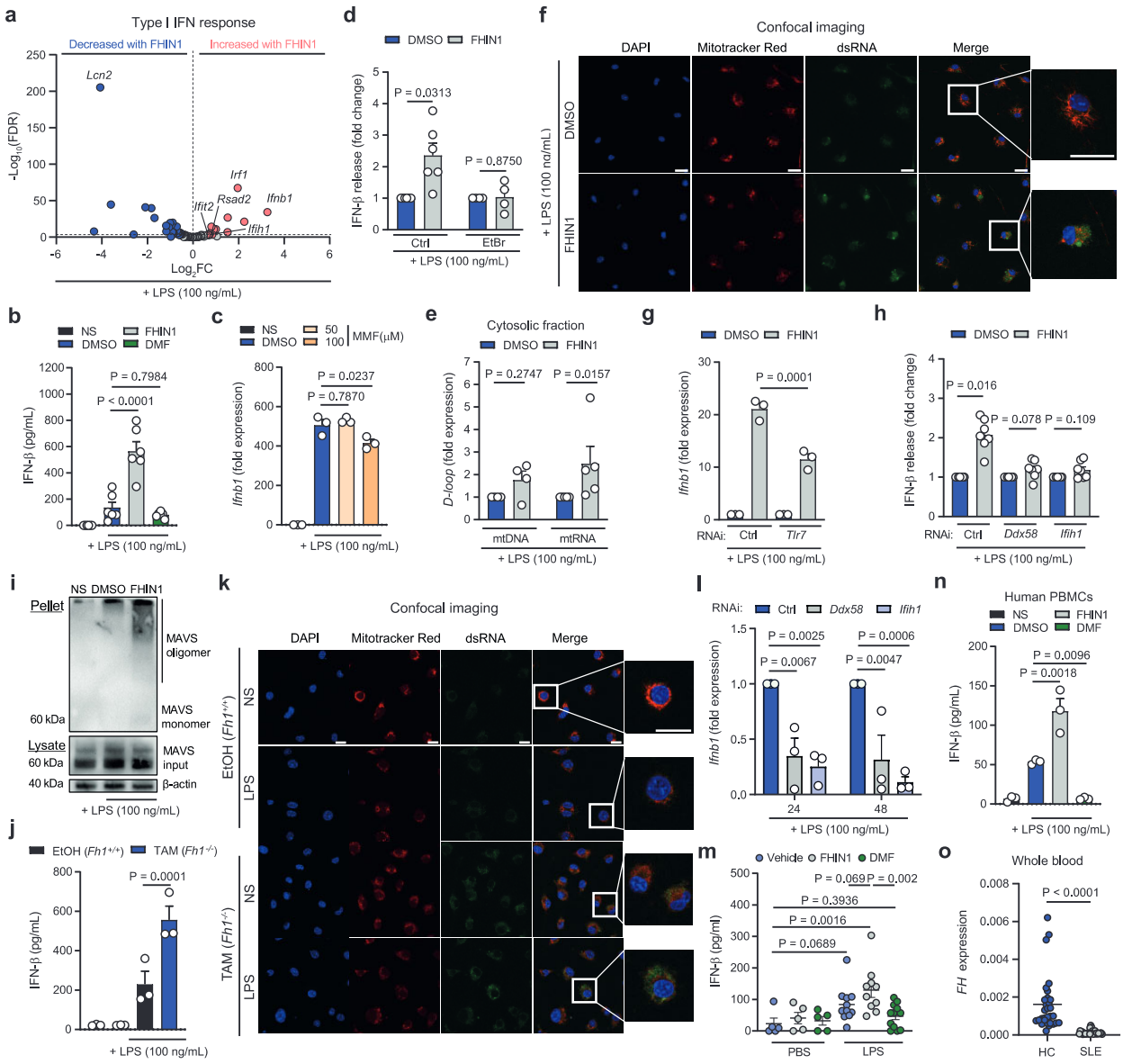
a
Type I IFN response
Decreased with FHIN1
Increased with FHIN1
-Log10(FDR)
Log2FC
Lcn2
Irf1
Rsad2
Ifnb1
Ifit2
Ifih1
+ LPS (100 ng/mL)
d
DMSO FHIN1
IFN-β release (fold change)
P = 0.0313
P = 0.8750
Ctrl
EtBr
+ LPS (100 ng/mL)
f
Confocal imaging
DAPI
Mitotracker Red
dsRNA
Merge
DMSO
FHIN1
+ LPS (100 ng/mL)
b
NS
DMSO
FHIN1
DMF
IFN-β (pg/mL)
P = 0.7984
P < 0.0001
+ LPS (100 ng/mL)
c
NS
DMSO
50
100
MMF(μM)
Ifnb1 (fold expression)
P = 0.0237
P = 0.7870
+ LPS (100 ng/mL)
e
Cytosolic fraction
DMSO FHIN1
D-loop (fold expression)
P = 0.2747
P = 0.0157
mtDNA
mtRNA
+ LPS (100 ng/mL)
g
DMSO FHIN1
Ifnb1 (fold expression)
P = 0.0001
RNAi: Ctrl Tlr7
+ LPS (100 ng/mL)
h
DMSO FHIN1
IFN-β release (fold change)
P = 0.016
P = 0.078
P = 0.109
RNAi: Ctrl Ddx58 Ifih1
+ LPS (100 ng/mL)
i
NS DMSO FHIN1
Pellet
MAVS oligomer
MAVS monomer
60 kDa
Lysate
60 kDa
MAVS input
40 kDa
β-actin
+ LPS (100 ng/mL)
k
Confocal imaging
DAPI
Mitotracker Red
dsRNA
Merge
EtOH (Fh1+/+)
TAM (Fh1-/-)
NS
LPS
l
RNAi: Ctrl Ddx58 Ifih1
Ifnb1 (fold expression)
P = 0.0025
P = 0.0006
P = 0.0067
P = 0.0047
24
48
+ LPS (100 ng/mL)
n
Human PBMCs
NS
DMSO
FHIN1
DMF
IFN-β (pg/mL)
P = 0.0096
P = 0.0018
+ LPS (100 ng/mL)
j
EtOH (Fh1+/+)
TAM (Fh1-/-)
IFN-β (pg/mL)
P = 0.0001
+ LPS (100 ng/mL)
m
Vehicle
FHIN1
DMF
IFN-β (pg/ml)
P = 0.069
P = 0.002
P = 0.3936
P = 0.0016
P = 0.0689
PBS
LPS
o
Whole blood
FH expression
P < 0.0001
HC
SLE